HHS Public Access

Author manuscript

Cell Metab. Author manuscript; available in PMC 2018 September 05.

Published in final edited form as:

Cell Metab. 2017 September 05; 26(3): 475–492.e7. doi:10.1016/j.cmet.2017.08.008.

A Stat6/Pten axis links cold exposure with T cell tolerance in adipose tissue

Stefanie Kälin[1,2,#], **Maike Becker**[2,3,#], **Verena B. Ott**[1,2], **Isabelle Serr**[2,3], **Fabian Hosp**[4], **Mohammad M. H. Mollah**[2,3], **Susanne Keipert**[1,2], **Daniel Lamp**[1,2], **Francoise Rohner-Jeanrenaud**[5], **Victoria K. Flynn**[2,3], **Martin G. Scherm**[2,3], **Lucas F. R. Nascimento**[2,3], **Katharina Gerlach**[6], **Vanessa Popp**[6], **Sarah Dietzen**[7], **Tobias Bopp**[7], **Purna Krishnamurthy**[8], **Mark H. Kaplan**[8], **Manuel Serrano**[9], **Stephen C. Woods**[10], **Philipp Tripal**[11], **Ralf Palmisano**[11], **Martin Jastroch**[1,2], **Matthias Blüher**[12], **Christian Wolfrum**[13], **Benno Weigmann**[7], **Anette-Gabriele Ziegler**[2,14], **Matthias Mann**[4], **Matthias H. Tschöp**[1,2,*], and **Carolin Daniel**[3,2,*]

[1]Institute for Diabetes and Obesity, Helmholtz Diabetes Center at Helmholtz Zentrum München and Division of Metabolic Diseases, Technische Universität München, 85748 Munich, Germany [2]Deutsches Zentrum für Diabetesforschung (DZD), 85764 Munich, Germany [3]Institute for Diabetes Research, Young Investigator Group Immune Tolerance in Type 1 Diabetes, Helmholtz Diabetes Center at Helmholtz Zentrum München, 80939 Munich, Germany [4]Max Planck Institute of Biochemistry, 82152 Martinsried, Germany [5]Laboratory of Metabolism, Division of Endocrinology, Diabetology, Hypertension and Nutrition, Department of Internal Medicine Specialties, Faculty of Medicine, University of Geneva, Geneva, Switzerland [6]Department of Medicine 1, University of Erlangen-Nuremberg, 91052 Erlangen, Germany [7]Institute of Immunology, Johannes Gutenberg University, 55131 Mainz, Germany [8]Indiana University School of Medicine, HB Wells Center for Pediatric Research, IN 46202, USA [9]Tumour Suppression Group, Spanish National Cancer Research Centre (CNIO), 28029 Madrid, Spain [10]Dept. of Psychiatry, University of Cincinnati, USA [11]OICE (Optical Imaging Centre Erlangen), University

[*]Corresponding authors: Carolin Daniel, PhD, Helmholtz Zentrum München, German Research Center for Environmental Health, Institute of Diabetes Research, Group Immune Tolerance in Diabetes, Heidemannstraße 1, 80939 München, phone: +49 89 3187 2188, fax: +49 89 3187 3144, carolin.daniel@helmholtz-muenchen.de. Matthias H. Tschöp, M.D., Director, Helmholtz Diabetes Center & Helmholtz Pioneer Campus, Institute for Diabetes and Obesity at Helmholtz Zentrum München, Chair, Division of Metabolic Diseases, Department of Medicine, Technische Universität München, T +49(0)89 3187-2103, M tschoep@helmholtz-muenchen.de, HelmholtzZentrum München, Business Campus Garching-Hochbrück, Parkring 13, 85748 Garching, Germany.
[#]both authors contributed equally to this work.

Competing interests: None.

Author contributions

SK and MB performed *ex vivo*, *in vitro* and *in vivo* experiments analyzed data and wrote the manuscript. VBO performed *in vitro* T cell analyses and qPCR analyses of adipose tissue function. IS performed *in vivo* experiments in humanized mice. LRN performed *in vitro* experiments for analyses of fat-residing $CD4^+$T cells. MoM analyzed mitochondrial membrane potentials. VKF and MB performed human *in vitro* experiments. MGS performed Treg induction analyses. SuK supported analyses of BAT function. DL supported functional analyses of T cells. FRJ provided betaless mice and supported analyses of animals. KG and VP isolated and analyzed T cells. MK provided Stat6VT mice and supported analyses of mice. MJ supported analyses of BAT tissues. FH performed proteomic profiling of $CD4^+$T cells. MS provided PtenTg mice and supported analyses of animals. MatB supported analyses of adipose tissue function. TB provided Foxp3 DTR mice. CW performed experiments with *in vivo* cold exposure. PT and RP performed STED microscopy and related analyses. BW performed gain and loss of function experiments for Treg analyses, immunofluorescence and confocal microscopy. SCW contributed to the writing of the manuscript. AGZ is PI of the Munich Bioresource project and provided blood samples from healthy individuals. MM supported and supervised proteomic analyses. MHT provided substantial contribution to conceptualization and discussion of the project and contributed to writing of the manuscript. CD conceptualized, designed, performed *in vivo* experiments with humanized mice, analyzed and interpreted data and wrote the manuscript.

Erlangen, 91052 Erlangen, Germany [12]University of Leipzig, Department of Medicine, Research Group Molecular Endocrinology, 04103 Leipzig, Germany [13]Institute of Food, Nutrition and Health, ETH Zurich, 8603 Schwerzenbach, Switzerland [14]Institute for Diabetes Research, Helmholtz Diabetes Center at Helmholtz Zentrum München, 80939 Munich and Klinikum rechts der Isar, Technische Universität München, 80333 Munich, Germany

Summary

Obesity and type-2 diabetes are associated with tissue-inflammation and metabolic defects in fat depots. Foxp3^{+}regulatory T(Treg) cells mediate T-cell tolerance, thereby controlling tissue inflammation. However, the molecular underpinnings how environmental stimuli interlink T-cell tolerance with adipose tissue function remain largely unknown. Here, we report that cold exposure or beta3-adrenergic receptor (ADRB3) stimulation induces T-cell tolerance *in vitro* and in murine and humanized models. Tolerance induction was verified by CD4^{+}T-cell-proteomes revealing higher protein expression of Foxp3 regulatory networks. Specifically, Ragulator-interacting protein C17orf59, which limits mTORC1 activity, was upregulated by either ADRB3-stimulation or cold-exposure, and therefore might enhance Treg induction. By loss and gain-of-function studies, including Treg depletion and transfers *in vivo*, we demonstrated that a T-cell-specific Stat6/Pten axis links cold-exposure or ADRB3 stimulation with Foxp3^{+}Treg induction and adipose tissue function. Our findings open new avenues in understanding tissue-specific T-cell tolerance and the design of precision concepts toward personalized immune-metabolic health.

TOC Blurb

Inflammatory processes in metabolically active tissues are believed to contribute to the development of obesity and type-2 diabetes. We here report that immunesuppressive regulatory T cells represent key components of the molecular interface connecting environmental influences with functional integrity of adipose tissue in mice and men. Specifically, we find that a T cell-specific Stat6/Pten signaling axis links cold exposure or adrenergic stimuli with regulatory T cell activity and adipose tissue function, offering novel molecular approaches toward personalized immune-metabolic health.

Introduction

Obesity and type-2 diabetes (T2D) represent one of the most severe health threats of modern society. Although inflammation is critically associated with obesity and T2D (Hotamisligil, 2006), the functional interplay between adipose tissue and immune cells remains incompletely understood. Adipocytes can be divided into classes of white, brown and beige cells (Kissig et al., 2016; Rosen and Spiegelman, 2014). Metabolic disease is differentially associated with local fat depots, with visceral white adipose tissue (visWAT) being especially prone to obesity-associated inflammation (Rosen and Spiegelman, 2014). Adipocytes are surrounded by several immune cell types (Kanneganti and Dixit, 2012; Mathis, 2013), and there is evidence that crosstalk between adipose and immune cells is important during cold exposure (Qiu et al., 2014).

Recently a critical function of fat-residing effector and regulatory $CD4^+$T lymphocytes in adipose-immune crosstalk has been reported (Bapat et al., 2015; Cipolletta et al., 2012; Feuerer et al., 2009). In particular, a subset of $Foxp3^+$regulatory T (Treg) cells was identified to have a pivotal role for the maintenance of visWAT homeostasis (Cipolletta et al., 2012; Feuerer et al., 2009; Mathis, 2013). Tregs mediate T cell tolerance and are important to control immune inflammation locally. Orchestration of the Treg population residing in visWAT is carried out in part by PPAR-γ (Cipolletta et al., 2012; Panduro et al., 2016). PPAR-γ collaborates with Foxp3 to impose the transcriptional profile characteristic of visWAT Tregs on naïve $CD4^+$T cells (Cipolletta et al., 2012).

Immune cell type, numbers and function dramatically change in visWAT in response to overnutrition. Specifically, Treg frequencies are severely reduced and are accompanied by increased inflammation. One study reported that brown adipose tissue (BAT) from female C57Bl/6 mice hosts Tregs with a transcriptome different from that of their splenic counterparts (Medrikova et al., 2015). However, in spite of multiple studies examining T cell responses in visWAT, our understanding of Treg function in subcutaneous white adipose tissue (scWAT) and BAT remains limited.

To interfere with metabolic impairments in obesity, cold exposure has gained considerable interest as one major determinant of energy expenditure, as recent studies uncovered cold-inducible BAT in adult humans (Cypess et al., 2013; Saito et al., 2009). This is important since cold acclimation is known to provide beneficial effects on whole-body and skeletal muscle insulin sensitivity in patients with obesity and T2D (Hanssen et al., 2015). Intense research efforts have therefore focused on stimulating BAT energy expenditure through activation of the beta3-adrenergic receptor (ADRB3), which is expressed on human adipocytes and other tissues including human peripheral blood mononuclear cells (Cypess et al., 2013; Yu et al., 2007). Recently, the ADRB3 agonist mirabegron (Malik et al., 2012; Takasu et al., 2007) was reported to stimulate human BAT thermogenesis (Cypess et al., 2015).

In order to interfere with inflammatory conditions, cold exposure or short term cryostimulation presumably activates the same ADRB3 and have been implemented in clinical settings e.g., in rheumatoid arthritis or multiple sclerosis (Guillot et al., 2014). Preliminary studies indicated an increase in anti-inflammatory cytokine production upon short-term cryostimulation (Klimek et al., 2011; Lubkowska et al., 2011).

However, it remains unknown whether cold exposure or adrenergic signals might modulate local adaptive immune responses such as effector and regulatory $CD4^+$T cells. Additionally, insights into the mutual crosstalk between local T cells and adipose tissue, especially in BAT and scWAT remain limited. Such insights into the role of tissue-specific Treg induction and function will be critical for the development of precision interventions limiting tissue-specific inflammation to support adipose tissue function.

Here, we report that environmental stimuli such as cold exposure or ADRB3 stimulation induce T cell tolerance *in vitro* and in murine and humanized *in vivo* models. Diet-induced thermogenesis by short-term exposure to a high-caloric challenge likewise increased

Foxp3^{+}Treg frequencies and induction in BAT. We used CD4^{+}T cell proteomes to demonstrate tolerance induction and higher protein expression of Foxp3 regulatory networks. Specifically, the Ragulator-interacting protein C17orf59, which limits mTORC1 activity, was upregulated by both ADRB3 stimulation and cold exposure, and therefore might enhance Treg induction. Using a series of T-cell-specific and adipose-related loss and gain of function studies, including Treg depletion, transfers, and expansion *in vivo*, we demonstrated that a T cell-specific Stat6/Pten axis links cold exposure or ADRB3 stimulation with Foxp3^{+}Treg induction and adipose tissue function.

Results

BAT and scWAT harbor more CD4^{+}CD25^{+}Foxp3^{+}Tregs than visWAT

To investigate frequencies, functional characteristics and induction of Foxp3^{+}Tregs from different fat depots we used young lean Balbc Foxp3 GFP reporter mice (3–6 weeks of age). A set of exclusion markers permitted the direct identification of a CD4^{+}T cell subset purified from three fat depots (Fig. 1A). The percentages of locally-residing Foxp3 GFP^{+}Tregs purified from fat depots of young lean animals were higher in BAT and scWAT than in visWAT (Tregs in BAT vs. visWAT, P=0.0015; Tregs in scWAT vs. visWAT, P=0.0003, Fig. 1B+C). We likewise identified higher ratios of human Foxp3/CD4 mRNA in scWAT from lean individuals when compared to their visWAT (Figure S1A).

Treg induction is more efficient in T cells from BAT and scWAT than from visWAT

Next, to determine Foxp3^{+}Treg induction capacities in accordance with their localization in different fat depots, we purified naïve CD4^{+}CD44^{low}CD25^{-}Foxp3GFP^{-}T cells from BAT, scWAT and visWAT of Balbc Foxp3 GFP reporter mice. Our findings are in line with recently emerging evidence demonstrating the presence of naïve CD4^{+}CD25^{-}T cells in various non-lymphoid tissues (Kim, 2007; Lewis et al., 2008). For *in vitro* Treg induction, we used protocols mimicking subimmunogenic T cell receptor (TCR) stimulation without TGFβ and premature withdrawal of TCR stimulation (Sauer et al., 2008; Serr et al., 2016). We compared *in vitro* Treg induction capacities between naive CD4^{+}CD25^{-}CD44^{low}Foxp3GFP^{-} T cells from different fat depots. Treg induction was most efficient using naïve T cells purified from BAT and scWAT (induced CD4^{+}CD25^{+}Foxp3^{high} Tregs [% of CD4^{+}T cells] BAT: 26.5±0.6 vs. scWAT: 16.0±0.9; Fig. 1D+E). Significantly lower frequencies of induced Foxp3^{+}Tregs were obtained when naïve CD4^{+}T cells from visWAT were used (induced CD4^{+}CD25^{+}Foxp3^{high} Tregs [% of CD4^{+}T cells] visWAT: 9.6±0.9, P<0.01, Fig. 1D–F). Optimal Foxp3^{+}Treg induction was found to require the subimmunogenic delivery of strong-agonistic TCR ligands to naïve CD4^{+}T cells (Daniel and von Boehmer, 2011; Daniel et al., 2011; Gottschalk et al., 2010). The most efficient *de novo* Foxp3^{+}Treg induction is achieved in those T cells that proliferate the least (Kretschmer et al., 2005). We observed a lower proliferative potential in T cells from BAT and scWAT when compared to visWAT (CD4^{+}Ki67^{+}T cells (mean fluorescence intensity (MFI)) BAT: 2050±50 vs. scWAT: CD4^{+}Ki67^{+}T cells: 3025±75 vs. visWAT: CD4^{+}Ki67^{+}T cells: 4235±45, P<0.01, Fig. S1B).

We next asked whether these different adipose tissue environments would likewise infer metabolic programs onto local T cells and affect their differentiation and function. $CD4^+$T cells purified from BAT and scWAT of lean mice harbored significantly decreased percentages of depolarized mitochondria when compared to cells from visWAT (Fig. S1C). These data support the notion that $CD4^+$T cells residing in BAT and scWAT possess a lower glycolytic activity than visWAT derived T cells. This observation is consistent with the lower proliferative potential of BAT and scWAT-derived T cells (Fig. S1B) and their higher *de novo* Treg induction potential (Fig. 1E+F).

Cold exposure enhances Treg induction in adipose tissue T cells

Since brown/beige fat thermogenesis is stimulated by environmental cold, we next investigated the effects of cold exposure on local Treg frequencies and induction (staining examples are in Fig. S1D). Cold acclimation (1 wk at 8°C) significantly increased frequencies of $Foxp3^+$Tregs purified from inguinal lymph nodes of mice (Fig. 1G+H). Importantly, short-term cold acclimation (24 h at 4°C) likewise induced a significant enhancement of $Foxp3^+$Tregs in T cells from BAT, scWAT and visWAT ($CD4^+CD25^+Foxp3^+$T cells [% of $CD4^+$T cells] BAT: 7.4±0.6 vs. BAT after cold: 11.6±0.8, $P<0.001$; scWAT: 7.2±0.2 vs. scWAT after cold: 15.9±0.6, $P<0.001$, visWAT: 4.9±0.3 vs. visWAT after cold: 8.8±0.4, $P<0.001$, Fig. 1I). When we purified naïve $CD4^+$T cells from respective fat depots after 24 h of cold and subjected them to *in vitro* Treg induction assays, Treg induction capacities were significantly enhanced ($CD4^+CD25^+Foxp3^+$T cells [% of $CD4^+$T cells] BAT: 32.5±1.2 vs. BAT after cold: 61.1±2.2, $P<0.01$; scWAT: 30.3±3.2 vs. scWAT after cold: 43.3±2.4, $P=0.0098$; visWAT: 11.9±0.5 vs. visWAT after cold: 24.4±1.6, $P<0.001$, Fig. 1J)

Beta-adrenergic stimulation enhances Treg induction *in vitro*

The data on Treg induction of fat-residing T cells upon cold-exposure prompted us to investigate the role of ADRB3 agonists on local T cell tolerance. Previous studies as well as *in silico* analyses (Heng et al., 2008) suggested expression of *Adrb3*, which encodes for the beta-3 adrenergic receptor, in human and murine lymphocytes (Yu et al., 2007). Accordingly, we found low mRNA expression levels of *Adrb3* in murine $CD4^+$T cells (Fig. S1E).

ADRB3 stimulation induces Tregs *in vitro*

When we next tested the specific ADRB3 agonist CL-316243 (CL) for Treg induction *in vitro* using naïve $CD4^+$T cells from Balbc Foxp3 GFP reporter mice, it became clear that at low picomolar doses, the ADRB3 agonist significantly enhances Treg induction ($CD4^+CD25^+Foxp3^+$T cells [% of $CD4^+$T cells] control: 35.9±0.7 vs. + CL [0.01 nM]: 45.1±1.0, $P<0.001$, Fig. S1F+G). Likewise, in naïve $CD4^+$T cells purified from respective fat depots of young Balbc mice, low-dose CL-treatment enhanced Treg induction most efficiently in T cells from BAT and scWAT as compared to visWAT (Fig. S1H+I). Higher non-subimmogenic concentrations of ADRB3 agonists can promote cellular proliferation thereby reducing Treg induction efficacy from naïve $CD4^+$T cells.

ADRB3 blockade reduces Treg induction *in vitro* and *in vivo*

CL-mediated increased Treg induction was reduced by co-incubation with an ADRB3 antagonist (cyanopindolol (Cya)) ($CD4^+CD25^+Foxp3^+$T cells [% of $CD4^+$T cells] +CL [0.001 nM]: 23.3±0.8 vs. + CL [0.001 nM] +Cya [0.1 nM]: 16.7±0.5, $P<0.001$, Fig. S1J). Moreover, *in vivo*, Treg induction potential was enhanced in naïve $CD4^+$T cells from CL-treated mice ($CD4^+CD25^+Foxp3^+$T cells [% of $CD4^+$T cells] BAT: 12.9±1.0 vs. BAT + CL *in vivo*: 21.0±0.8, $P<0.001$) and reduced upon co-treatment with an ADRB3 antagonist (Fig. S1K).

ADRB3 stimulation induces Treg cells *in vivo*

Application of an ADRB3 agonist to young Balbc Foxp3 GFP reporter mice *in vivo* (2 d at 1 mg/kg *i.p.*) enhanced Foxp3 expression in $CD4^+$T cells from inguinal lymph nodes and from fat (Fig. 2A–D; negative staining controls in Fig. S1L). Treg induction with naïve $CD4^+$T cells was most prominently increased in T cells isolated from BAT and scWAT as compared to visWAT (Fig. 2E).

ADRB3 stimulation induces human T cell tolerance *in vitro* and in humanized mice

Limited TCR stimulation *in vitro* (Sauer et al., 2008; Serr et al., 2016) in the presence of low doses of the human ADRB3 agonist mirabegron significantly enhanced human Treg induction ($CD25^{++}Foxp3^{high}$ [% of $CD127^{low}CD25^{++}CD4^+$T cells]: control: 46.6±1.1 vs. +Mira [0.1 nM]: 59.3±0.6, $P<0.001$, Fig. S2A).

To assess *in vivo* relevance, we investigated human Treg induction in humanized NSG mice in accordance with previously established procedures (Serr et al., 2016) (Fig. S2B). Humanized mice were treated with mirabegron for 3 d (1 mg/kg, *i.p.*) which significantly increased frequencies of human $CD4^+CD127^{low}CD25^{high}$Tregs ($CD4^+CD127^{low}CD25^{high}$Tregs [% of $CD4^+$T cells]: control: 1.9±0.5 vs. +Mira: 4.9±1.0, $P=0.0319$, Fig. S2B+C). Moreover, purified naïve human $CD4^+$T cells from mirabegron-treated humanized animals had improved Treg-induction capacities *in vitro* (Fig. S2C–G).

T cell tolerance is impaired in the absence of beta-ARs *in vivo*

To mechanistically dissect these findings, we next analyzed mice lacking all three beta-adrenergic receptors (Bachman et al., 2002) and observed significantly decreased Treg frequencies in inguinal lymph nodes and subcutaneous fat depots (Fig. 2F–H). As one possible means to explain this reduced Treg abundance in comparison to WT mice, $Foxp3^+$Tregs residing in scWAT of betaless mice showed significantly reduced proliferative potential as assessed by Ki67 expression (Fig. S2H). Likewise, Treg induction potential using naïve $CD4^+$T cells from fat depots of betaless mice was reduced when compared to WT animals (Fig. 2I). Treg induction assays using naïve $CD4^+$T cells from betaless mice and ADRB3 agonists or antagonists indicated no effect on tolerance induction (Fig. S2I).

ADRB3-stimulation-induced Tregs are required for adipose tissue function

To investigate the importance of Tregs in adipose tissue function upon ADRB3 stimulation *in vivo,* we next performed loss-of-function experiments. ADRB3 stimulation *in vivo* (CL

for 3 d at 1 mg/kg, *i.p.*) induces genes relevant for BAT function (Fig. S3A). In a first set of loss-of-function studies, Tregs were depleted in Balbc Foxp3 GFP reporter mice prior to the start of ADRB3 stimulation by the use of established procedures involving anti-CD25 antibody application (Setiady et al., 2010) (Fig. 3A). Treg-depleted mice (control stainings for efficacy of Treg depletion in adipose tissue in Fig. S3B) and control animals were injected with CL (3 d at 1 mg/kg, *i.p.*). In control mice without Treg depletion, thermogenic genes (*Ucp1, Ppargc1a, Prdm16* and *Cidea*) were induced in BAT after ADRB3 agonist treatment. This induction by ADRB3 stimulation was blunted in mice with Treg depletion (Fig. 3C). Accordingly, upon ADRB3 stimulation, we found the β-oxidation genes (*Acox1* and *Ascl1*) as well as lipolysis-related genes (*Lpl*, *Lipe*) to be upregulated in BAT, and again, this induction was not seen in mice with depleted Tregs (Fig. 3C). Moreover, in contrast to control mice treated with ADRB3 stimuli *in vivo*, BAT tissue of Treg-depleted CL-treated mice had significantly increased *Il6* (Fig. 3C). Further analyses of BAT tissue revealed a significant decline of *Plin1*, *Cycs*, *P2rx5*, *Glut1* and *Adipoq* in Treg-depleted CL-treated mice (Fig. S3C) thereby underlining a role of Foxp3^{+}Tregs in regulating lipolysis and thermogenesis in BAT. In a second set of loss-of-function studies, we used C57Bl/6 Foxp3 DTR mice (Kim et al., 2007) and diphtheria toxin-mediated Treg depletion to confirm the results seen from Treg-depleted animals using anti-CD25 antibodies. Accordingly, upon ADRB3 stimulation Treg-depleted Foxp3 DTR mice (Fig. 3B+D) exposed to cold (4°C for 24 h) had a significant reduction in thermogenic genes including *Ucp1*, *Ppargc1a*, and *Cidea* and in β-oxidation genes such as *Acsl1* in BAT while *Il6* levels mildly increased (Fig. 3D, control stainings for Treg depletion in Fig. S3D). Treg loss of function likewise mildly impacted scWAT function accompanied by a decline in *Pparg*, *P2rx5*, *Cidea* and *Lipe* (Fig. 3E). Moreover, in visWAT, upon DT-mediated Treg depletion and cold exposure we found expression levels of *Adipsin*, *Pparg*, *Ppargc1a*, *P2rx5*, *Plin1* and *Lipe* to be decreased while *Il6* was significantly upregulated (Fig. 3F).

Foxp3^{+}Tregs regulate adipose tissue function

Next, to directly assess the role of Foxp3^{+}Tregs in regulating adipose tissue function, we performed gain-of-function experiments by *in vivo* transfers of Foxp3GFP^{+}Tregs into respective Balbc recipient mice (*i.v.* or *i.p.* transfer). First, analyses of BAT function one wk after transfer revealed a significant enhancement of thermogenic genes (*Ucp1*, *Adrb3*, *Ppargc1a*, *Prdm16* and *Cidea*) in BAT (Fig. 3G). Consistent with this, we found increased levels of mRNA of β-oxidation genes (*Acox1* and *Ascl1*) as well as of lipolysis-related genes (*Lpl*, *Lipe*) in BAT after Treg transfer (Fig. 3G). Additionally, we observed *Plin1*, *Cycs*, *P2rx5*, *Glut1* and *Adipoq* to be enhanced in BAT tissue upon Treg transfer (Fig. S4A). Mild changes upon Treg transfer were also seen in scWAT tissue with *Ppara*, *Prdm16*, *Cpt1b* and *Glut1* being upregulated (Fig. S4B). The Treg-mediated improvement of BAT function (thermogenic capacity and lipolytic function) upon Treg transfer (Fig. 3G) was equal, or partially superior to, what occurred with ADRB3 agonist treatment *in vivo.*

To more specifically address the impact of Foxp3^{+}Tregs in modulating white adipose tissue function we employed *in situ* expansion of Foxp3^{+}Treg cells using subcutaneous injections of IL-2–mAb complexes (3 d, 6 μg per injection, *s.c.*) as a second gain-of-function model. These complexes cause a selective expansion of Foxp3^{+}Treg cells (Daniel et al., 2010;

Webster et al., 2009). Upon Foxp3$^+$Treg expansion we found a significant enhancement of thermogenic genes (*Ucp1*, *Ppargc1a*, *Prdm16* and *Cidea)* in scWAT, accompanied by increased levels of β-oxidation (*Acox1 and Acsl1*) and lipolysis-related genes (e.g. *Lipe* and *Plin1*, Fig. S4C+D), together with an increased expression of *P2rx5, Pparg, Ppara* and *Adipsin*.

Gain-of-function experiments by Treg expansion also mildly impacted visWAT metabolic function. Specifically, we observed upregulation in genes related to differentiation (*Pparg* and *Adipsin*), browning (*Cd137*) as well in genes related to lipolysis (*Acox1, Lipe, Lpl, Plin1*) (Fig. S4E). In addition to the upregulation seen for *Pparg* and *P2rx5* following Treg gain-of-function, the significant increase in *Adipsin* expression seen in BAT, scWAT and visWAT upon Treg expansion further point to an impact of Foxp3$^+$Tregs in regulating adipocyte differentiation (Fig. S4F).

Local Foxp3$^+$Treg induction is impaired in the absence of UCP1

The thermogenic activity of brown fat cells relies, to a great extent, on uncoupling protein 1 (UCP1), a protein that is localized on the inner membrane of mitochondria. Upon activation, UCP1 catalyzes the leak of protons across the mitochondrial membrane (Fedorenko et al., 2012), which uncouples oxidative respiration from ATP synthesis while the resulting energy derived from substrate oxidation is dissipated as heat. To further dissect the question, whether the fat thermogenic response causes Treg activation or whether Treg activity is required for thermogenic responses we used UCP1-ablated (UCP1ko) mice. The percentages of locally-residing CD4$^+$CD25$^+$Foxp3$^+$Tregs purified from fat depots of young UCP1ko mice were reduced in BAT and scWAT while marginal or no changes were seen in visWAT (Fig. S5A+D). Likewise, *de novo* Treg induction was lower in naïve CD4$^+$CD25$^-$T cells purified from BAT and scWAT of UCP1ko mice when compared to WT T cells (Fig. S5B +E). The reduced Treg percentages and their lower Treg induction potential were accompanied by a higher proliferative potential in local CD4$^+$CD25$^-$T cells from UCP1ko mice when compared to littermates (Fig. S5C,F,G), both *ex vivo* and upon TCR stimulation during Treg induction *in vitro*. These data support the notion of a mutual crosstalk between immune cells and adipose tissue in that the local tissue environment impacts T cell differentiation and function, which in turn can influence tissue function and organismal homeostasis (Panduro et al., 2016).

Pathological activation of adipose tissue by exposure to high-caloric challenge differentially affects Foxp3$^+$Tregs in BAT, scWAT vs. visWAT

To examine pathological environmental conditions in which these pathways are activated we focused on high-caloric challenge by exposure to high fat/high sugar (HFHS) diet. High-caloric diets were demonstrated to also induce BAT thermogenesis (Rothwell and Stock, 1979), which was shown to depend on UCP1 function (Feldmann et al., 2009).

A 2 wk challenge of HFHS diet to 6 wk-old Bl6 Foxp3 GFP reporter mice or 8 wk-old Balbc Foxp3 GFP reporter mice resulted in a significant enhancement of CD4$^+$Foxp3GFP$^+$Tregs residing in BAT (Fig. S6A+B). Mild changes in Treg percentages were seen in scWAT, while the short-term high-caloric challenge resulted in a significant

decline in Treg percentages in visWAT (Fig. S6A+B). An exposure to HFHS diet for 8 wk did not alter Treg ratios in BAT and scWAT of B6 Foxp3 GFP reporter mice; in accordance with earlier studies (Cipolletta et al., 2015; Cipolletta et al., 2012) indicating local Treg expansion in visWAT in this age group (~14 weeks of age), we found higher ratios of Tregs during standard diet. In contrast to Tregs residing in BAT and scWAT Tregs in visWAT were severely reduced by exposure to HFHS diet (Fig. S6C). Long term exposure to HFHS diet for 16 wk left $CD4^+CD25^+Foxp3^+$Tregs in BAT unaltered and only mildly reduced them in scWAT of Balbc mice, while $Foxp3^+$Tregs in visWAT were significantly reduced by high-caloric challenge (Fig. S6D).

In accordance with the increase seen in BAT-residing Tregs seen upon a 2 wk HFHS diet challenge, Treg induction potential of naïve $CD4^+$T cells was likewise significantly enhanced (Fig. S6E–G).

To address the question whether a diet-induced thermogenic response causes Treg activation or whether Treg activity is required for responses in adipose tissue we again used a model of Treg depletion by anti-CD25 antibody application. Treg depletion prior to exposure to a 1 wk challenge of HFHS diet resulted in a significant decline in thermogenic genes in BAT such as *Ucp1, Ppargc1a, Pparg, Ppara* and *Prdm16* (Fig. S6H). Additionally, in Treg-depleted mice β-oxidation genes (*Ascl1*) as well as lipolysis-related genes (*Lipe*) were reduced. Furthermore, we found *Cycs*, *P2rx5* and *Adipsin* to be downregulated in BAT of Treg depleted mice (Fig. S6I). The responses seen upon Treg depletion and exposure to a HFHS diet in scWAT were more heterogeneous, while Treg depletion promoted a significant decline in *Pparg*, *Prdm16* and *Acsl1* (Fig. S6J).

Stat6 expression is higher in T cells from BAT and scWAT as compared to visWAT

Next, we aimed to identify potential signaling molecules that can impinge on the functional interplay between T cell tolerance induction and adipose tissue function. When comparing the gene expression patterns of murine $CD4^+$T cells from young Balbc Foxp3GFP reporter mice at room temperature in a pilot experiment, we observed higher levels of transcripts encoding the transcription factor *Stat6* in BAT compared to WAT (Fig. 4A).

Treatment with an ADRB3 agonist (2 d CL at 1 mg/kg *i.p.*) resulted in increased *Stat6* expression in $CD4^+$T cells (Fig. 4B; see quantification in Fig. S7A). Moreover, *in vivo* cold exposure induced *Stat6* mRNA expression in $CD4^+$T cells as assessed by RT-qPCR analyses (Fig. 4C). When we validated *Stat6* expression levels in fat-residing $CD4^+$T cells of Balbc Foxp3GFP reporter mice, we observed higher expression in $CD4^+$T cells from BAT when compared to scWAT or visWAT (Fig. 4D). *In vivo* cold exposure (4°C, 24 h) and ADRB3 stimulation (3 d CL at 1 mg/kg *i.p.*) likewise induced phosphorylation of Stat6 at position pY641 in $CD4^+$T cells from inguinal lymph nodes as seen from immunofluorescence analyses (Fig. 4E–G). Moreover, the percentage of cells that are p-Stat6-positive (and the MFI of the entire population) was increased in pre-activated $CD4^+$T cells after ADRB3 stimulation for 15 min *in vitro* (CL, 100 nM, Fig. 4H).

Stat6 has been implicated in exerting critical functions in promoting cold-induced remodeling of fat. For instance, cold-induced expression of *Ucp1* in scWAT was reported to

be severely decreased in *Stat6*−/− (Stat6ko) mice (Qiu et al., 2014). From an immunological perspective, Stat6 promotes Th2 and Th9 immunity (Goenka and Kaplan, 2011). However, recent studies pointed to a positive role for Stat6 as a second required signal in antigen-specific Treg induction (Chapoval et al., 2010; Pillemer et al., 2009; Sanchez-Guajardo et al., 2007), while in Stat6VT transgenic mice the constitutive activation of Stat6 increased the percentages of peripheral Tregs (Sanchez-Guajardo et al., 2007).

Induction of adipose tissue Tregs is impaired in the absence of Stat6

When we analyzed *ex vivo* Treg frequencies, as well as the Treg induction potential of naïve T cells purified from fat depots of BALB/c Stat6ko (Gessner et al., 2005; Kaplan et al., 1996) and WT animals, we observed local Treg ratios (BAT: $CD4^+CD25^+Foxp3^+$T cells [% of $CD4^+$T cells] WT: 10.5±0.7 vs. Stat6ko: 5.2±0.5, $P<0.001$; scWAT: WT: 7.7±0.9 vs. Stat6ko: 3.2±0.3, $P=0.0003$, Fig. 4I–K) and their induction to be significantly blunted in the absence of Stat6 ($CD4^+CD25^+Foxp3^+$T cells [% of $CD4^+$T cells]: BAT: WT: 26.1±1.0 vs. Stat6ko: 13.4±0.9, $P<0.001$; scWAT: WT: 16.0±0.9 vs. Stat6ko: 10.8±0.5, $P<0.001$, Fig. 4I–K).

In a second approach, a pharmacological Stat6 inhibitor significantly reduced Treg induction using naïve $CD4^+$T cells from inguinal lymph nodes of BALB/c Foxp3 GFP reporter mice (Fig. S7B).

Treg induction by ADRB3 stimulation requires Stat6

Treg induction using Stat6ko mice was unaffected by ADRB3 stimulation/blockade *in vitro* (Fig. S7C+D) or *in vivo* (CL 1 mg/kg, *i.p.*, 3 days, Fig. 4L). Since T cell-specific Stat6ko mice are not available for loss-of-function studies, we used *in vivo* T cell transfer experiments to assess T cell intrinsic effects relevant for Treg induction. We purified naïve $CD4^+$T cells from either WT or Stat6ko animals and transferred them into congenic BALB/c hosts to permit re-identification of transferred cells. In addition, mice were treated for 3 d with CL at 1 mg/kg, *i.p. in vivo*. Re-analysis of transferred cells revealed that in accordance with previous studies, Treg induction capacities *in vivo* in polyclonal TCR repertoires were low, although we found frequencies of induced Tregs to be significantly reduced in transferred T cells from Stat6ko mice ($CD4^+CD25^+Foxp3^+$T cells [% of $CD4^+$T cells] WT: 3.8±0.9 vs. Stat6ko: 1.5±0.3, $P=0.0200$, Fig. S7E). To dissect the question whether the impairment of T cell tolerance seen in fat depots of Stat6ko mice links with alterations in adipose tissue function, we next examined metabolic regulation in fat depots of Stat6ko mice upon ADRB3 stimulation *in vivo*. In contrast to WT mice (Fig. S3A), in Stat6ko mice ADRB3 stimulation *in vivo* (3 d CL, 1 mg/kg *i.p.*) did not increase genes important for BAT function (no upregulation was seen for *Ucp1*, *Ppargc1a*, *Cidea*, *Ascl1*, *Plin1*, *Lipe* and *P2rx5*), while ADRB3 stimulation in the absence of Stat6 significantly reduced mRNA abundance of *Pparg* ($p=0.0117$) and *Adipsin* ($P=0.0388$) (Fig. S7F). Genes related to thermogenesis, lipolysis and adipose differentiation were likewise unaffected by ADRB3 stimulation in scWAT from Stat6ko animals, while ADRB3 stimulation significantly reduced mRNA abundance of *Ucp1*, *Pparg*, *Lipe*, *Adipsin* and *P2rx5* in visWAT of Stat6ko mice (Fig. S7G, H).

In vivo Treg induction is enhanced in the presence of a constitutively active Stat6

In gain-of-function experiments, we used mice with a constitutively active Stat6 expressed in T cells (Bruns et al., 2003; Sehra et al., 2008) (Stat6VT$^+$ vs. Stat6VT$^-$ littermates). We identified increased frequencies of Foxp3$^+$Tregs in inguinal lymph nodes (CD4$^+$CD25$^+$Foxp3$^+$T cells [% of CD4$^+$T cells] Stat6VT$^-$: 11.7±0.5 vs. Stat6VT$^+$: 20.6±2.1, P=0.0007, Fig. 4M). *Ex vivo* Treg frequencies from adipose tissue of Stat6VT$^+$ mice showed a higher variability but were found to be increased when compared to Stat6VT$^-$ littermates (Fig. 4N).

Concerning adipose tissue function, in the steady state, without ADRB3 stimulation or cold exposure, Stat6VT$^+$ mice presented with increased mRNA abundance of *Pparg*, *Adipsin* and *P2rx5* in adipose tissue (Fig. S7I–K).

T cell tolerance in BAT is enhanced by Pten

Given the impairment of local tolerance induction in UCP1ko animals we next focused on Pten, which has been implicated in positively regulating BAT tissue function; e.g. by promoting *Ucp1* expression (Ortega-Molina et al., 2012). Animals with overexpression of *Pten* presented with a hyperactive BAT and harbored increased *Ucp1* levels in BAT (Ortega-Molina et al., 2012). Moreover, Pten has been critically implicated in the regulation of T cell tolerance (Sauer et al., 2008; Shrestha et al., 2015). We observed increased expression levels of *Pten* in CD4$^+$T cells purified from BAT and scWAT of Balbc mice (Fig. 5A). In accordance with the results seen for *Stat6* expression, *in vivo* cold exposure induced a significant increase in *Pten* expression levels of CD4$^+$T cells (Fig. 5B). In CD4$^+$T cells from inguinal lymph nodes of Stat6ko mice, we found *Pten* expression levels to be mildly downregulated when compared to WT animals (Fig. 5C).

As a gain-of-function approach we used *Pten* overexpressing animals (PtenTg). Such mice had significantly increased frequencies of Foxp3$^+$Tregs residing in inguinal lymph nodes, BAT and scWAT when compared to WT animals (BAT: CD4$^+$CD25$^+$Foxp3$^+$T cells [% of CD4$^+$T cells] WT: 9.6±0.2 vs. PtenTg: 12.7±0.2, P<0.001; scWAT: WT: 4.9±0.5 vs. PtenTg: 10.1±0.3, P<0.001; Fig. 5D+E). Moreover, the Treg induction potential was significantly enhanced in naïve CD4$^+$T cells of PtenTg animals (BAT: CD4$^+$CD25$^+$Foxp3$^+$T cells [% of CD4$^+$T cells] WT: 23.3±1.2 vs. PtenTg: 31.0±0.9, P=0.0010; scWAT: WT: 16.9±0.9 vs. PtenTg: 23.3±1.3, P=0.0052, Fig. 5F).

Levels of *Pten* overexpression varied in CD4$^+$T cells from PtenTg animals (~4 to ~40-fold). Mice with higher levels of *Pten* overexpression (~40-fold over WT) harbored significantly increased frequencies of Foxp3$^+$Tregs in all adipose tissues including visWAT (Fig. S7L).

No further increase in Treg induction *in vitro* was observed upon ADRB3 stimulation using naïve CD4$^+$T cells from PtenTg animals (Fig. 5G). In addition, ADRB3 stimulation *in vivo* (3d CL at 1 mg/kg *i.p.*) did not alter Treg frequencies in adipose tissue of PtenTg mice (Fig. 5H). Moreover, application of a Pten inhibitor significantly reduced Treg induction *in vitro* using naïve CD4$^+$T cells from inguinal lymph nodes of WT mice (Fig. 5I+J).

Cold exposure or ADRB3 stimulation *in vivo* induces a tolerogenic proteome signature in CD4$^+$T cells

Next, we used an unbiased approach to assess involved signaling pathways in CD4$^+$T cells upon cold exposure or low dose ADRB3 stimulation. To this end, we performed quantitative mass spectrometry-based proteomics (Meissner and Mann, 2014) to evaluate proteome compositions in CD4$^+$T cells upon *in vivo* cold acclimation of mice (8°C for one wk) or treatment with ADRB3 agonist (3 d CL at 1 mg/kg, *i.p.*). We identified 5,031 proteins in sorted CD4$^+$T cell proteomes of mice that were either exposed to cold or treated with CL *in vivo*, compared to control animals housed at room temperature or treated with NaCl, respectively. To verify tolerance induction upon cold exposure or ADRB3 stimulation *in vivo* at the protein level, we focused on proteins associated with selected GeneOntology terms Biological Function (GOBP) related to negative regulation of immune responses/ effector responses, as well as Treg induction and Foxp3 regulatory networks. Unsupervised hierarchical clustering conditions revealed up-regulation of several GO terms related to Treg induction upon cold exposure or ADRB3 stimulation *in vivo* among them Stat6 and Foxp3 (Fig. 6A+B). Similarly, several proteins of the Foxp3 regulatory network were found to be mildly up-regulated upon cold exposure or ADRB3 stimulation (Fig. 6C+D). Next, to address the relevance of Stat6 for linking ADRB3 stimulation with T cell tolerance induction in an unbiased setting we examined proteome compositions in CD4$^+$T cells from Stat6ko mice with or without ADRB3 stimulation *in vivo* (CL for 3 d at 1 mg/kg, *i.p.*). We identified 2,827 proteins in sorted CD4$^+$T cell proteomes of Stat6ko mice that were treated with CL *in vivo*, compared to control mice treated with NaCl, respectively. Unsupervised hierarchical clustering conditions showed that in the absence of Stat6 upon ADRB3 stimulation *in vivo* several GO terms related to Treg induction were rather downregulated, among them Foxp3 (Fig. 6G). Overall, these data highlight that in Stat6-competent animals either cold exposure or ADRB3 stimulation *in vivo* support a tolerogenic proteome signature in CD4$^+$T cells in accordance with identified increased Treg frequencies and the induction of Foxp3 regulatory networks (Fig. 6A–D).

ADRB3 stimulation or cold-exposure enhances fatty acid oxidation in CD4$^+$T cells

CD4$^+$T cells purified from mice that have been subjected to cold exposure or else treated with CL *in vivo* had upregulated proteins involved in enhancing fatty acid oxidation (FAO) such as Acsl4 and Cpt1a, as well as downregulation of proteins involved in negatively regulating FAO such as Acadvl and Acadl (Fig. 6A,B,E), thereby further supporting Treg induction and function (Chang and Pearce, 2016; MacIver et al., 2013; O'Sullivan and Pearce, 2015).

ADRB3 stimulation or cold-exposure increases C17orf59 protein expression in CD4$^+$T cells

Next, we combined both the cold/RT and the CL/NaCl datasets and performed pairwise comparison of the CD4$^+$T cells. Besides the mild upregulation of the Foxp3 regulatory network, we identified C17orf59 as one of the most prominently upregulated proteins in CD4$^+$T cells upon treatment with either ADRB3 agonist or cold *in vivo* (Fig. 6E for combined datasets, Fig. 6F for CL treatment only). C17orf59 was recently reported to function as a Ragulator-interacting protein that inhibits mTORC1 activity through its

interaction with Ragulator at the lysosome (Schweitzer et al., 2015). In accordance with previous studies (Daniel and von Boehmer, 2011; Sauer et al., 2008), inhibition of mTORC1 can directly enhance Foxp3$^+$Treg induction (Daniel et al., 2010).

C17orf59 was recently assigned a gene name, *BLOC-1 related complex subunit 6 (Borcs6).* *Borcs6* mRNA levels were significantly increased in CD4$^+$T cells from mice given ADRB3 stimulation (CL for 3 d at 1 mg/kg, *i.p.*], Fig. 6F). Consistent with the results upon ADRB3 stimulation, *Borcs6* mRNA levels were found to be enhanced following ADRB3 stimulation and cold exposure *in vivo* (Fig. 6H+I).

To validate the results by mass spectrometry we first used immunefluorescence for C17orf59 in CD4$^+$T cells together with confocal microscopy. We found C17orf59 protein expression to be upregulated following cold exposure or ADRB3 stimulation *in vivo* (Fig. 7A–D). Next, we employed stimulated emission depletion (STED) microscopy for creating super-resolution images in order to analyze expression changes of C17orf59 in cytoplasm of CD4$^+$T cells purified from inguinal lymph nodes of mice upon cold exposure in further detail (Fig. 7E). We found C17orf59 expression to be enhanced in CD4$^+$T cells from mice exposed to cold (24 h, 4°C) when compared to animals kept at RT (Fig. 7E). In line with the increased protein abundance of C17orf59 upon ADRB3 stimulation or cold exposure *in vivo* we dissected intracellular localization of mTOR in CD4$^+$T cells (Fig. 7F–H). While mTOR localizes more prominently to lysosomes in control CD4$^+$T cells, we found mTOR to remain more diffuse in T cells from mice that had received ADRB3 stimulation *in vivo* or were exposed to cold (Fig. 7F–H). Both ADRB3 stimulation and cold exposure resulted in significantly reduced frequencies of mTOR$^+$Lamp2$^+$CD4$^+$T cells (Fig. 7I+J). In addition, we provide first evidence that in the absence of Stat6 C17orf59 expression was reduced in the steady state when compared to WT mice (Fig. 7K, L, M).

Discussion

Here, we report the discovery of an important role of Treg cells in maintaining functional integrity of adipose tissue in response to environmental or systemic challenges. Specifically, in addition to cold exposure or physiological levels of beta-adrenergic stimulation we demonstrate that diet-induced thermogenesis by short-term exposure to a high-caloric challenge enhance T cell tolerance and their induction in BAT. This upregulation of thermogenesis-related genes upon short-term exposure to HFHS diet seen in BAT was blunted in Treg-depleted animals.

Furthermore, we find that local T cell tolerance induction was reduced in the context of impaired BAT-function using UCP1 ablated mice. We further reveal that a T cell-specific Stat6/Pten axis represents a mechanistic link between environmental challenges, induction of Foxp3$^+$Treg cells and immune-metabolic function in adipose tissue.

We examined loss- and gain-of-function studies, including Treg depletion, -transfer and *in vivo* expansion to demonstrate an important role of Foxp3$^+$Tregs for efficient thermogenesis and lipolysis. Furthermore, the results seen from *s.c.* Treg expansion *in vivo* underline a critical function of Foxp3$^+$Tregs in beiging/browning of white fat. Additionally, Treg gain-

of-function experiments enhanced expression of *Pparg*, *Adipsin* and *P2rx5* which was shown to be upregulated in differentiating brown adipocytes (Siegfried Ussar et al., 2014) and thereby suggest Foxp3$^+$Tregs as relevant players for adipocyte differentiation.

In order to dissect the question, whether the fat thermogenic response induces Treg activation or whether Treg activity is required for thermogenic responses we studied UCP1ko mice. We found Foxp3$^+$Treg frequencies and their induction in BAT to be reduced in the absence of UCP1. These results therefore support the notion of a mutual crosstalk between CD4$^+$T cells/Treg cells and adipose tissue. Specifically, these findings underline that the local adipose tissue environment can shape local T cell differentiation programs, which in turn can influence tissue function and organismal homeostasis.

Mechanistically, we provide evidence that Stat6 can function as one potential signaling molecule that impacts the functional interplay between T cell tolerance induction and adipose tissue function. The involvement of Stat6 in Foxp3$^+$Treg induction has been linked with the IL-2-Stat5 signaling pathway. IL-2R signals can induce IL-4 production through Stat5 (Zhu et al., 2003) or c-Maf activation (Hwang et al., 2002). The IL-4/Stat6/c-Maf/CD25 and IL-2/CD25/c-Maf/IL-4 pathways may converge to act on CD4$^+$CD25$^+$Foxp3$^+$Tregs (Sanchez-Guajardo et al., 2007). One means to explain the increase in peripheral Foxp3$^+$Tregs in mice with a constitutively-active Stat6 (Stat6VT$^+$ mice) might be an improved Treg cell survival by using common downstream elements of the IL-2 pathways (Sanchez-Guajardo et al., 2007). Additionally, IL-4, which promotes Stat6 activation (Quelle et al., 1995), can prevent apoptosis of CD25$^+$Foxp3$^+$Tregs (Maerten et al., 2005). It is hypothesized that in the periphery, Stat6 does not replace IL-2 signals, but rather acts in synergy to enhance Treg survival (Sanchez-Guajardo et al., 2007). Here, we show that fat-residing Treg abundance and induction, especially in BAT and scWAT, was critically impaired in the absence of Stat6.

Importantly, Stat6 is critically involved in regulating UCP1 expression in adipose tissue (Nguyen et al., 2011; Qiu et al., 2014). Furthermore, *in vivo* T cell transfer systems highlight the importance of T cell-specific *Stat6* expression in tolerance induction. ADRB3 agonist-mediated Treg enhancement was likewise not seen in the absence of Stat6. Accordingly, in contrast to WT mice in the absence of Stat6 upon ADRB3 stimulation *in vivo* we observed rather a downregulation of tolerogenic protein signatures including Foxp3. These immunological data on the reduction of T cell tolerance in Stat6 deficient animals integrate with metabolic analyses of fat depots from Stat6ko mice, which in contrast to WT mice upon ADRB3 stimulation *in vivo* showed a reduced expression of markers relevant for adipocyte differentiation such as *Pparg*, *P2rx5* and *Adipsin*. Together with the results seen from Treg gain- and loss-of-function studies these findings further support a role of Foxp3$^+$Tregs in impacting adipocyte differentiation.

As one possible means to further interlink Stat6-relevant signaling intermediates, mice with transgenic overexpression of *Pten* had decreased phosphorylated Akt as well as phosphorylated Foxo1 levels together with a significant enhancement of UCP1 expression in BAT (Ortega-Molina et al., 2012). Molecular analyses, including PI3K inhibitors, underscored that the effects of Pten on BAT are mediated by the PI3K/Akt/Foxo signaling

pathway that results in the activation of UCP1 and its transcriptional regulator Ppargc1a (Ortega-Molina et al., 2012).

The described metabolic effects on BAT function directly interlink with tolerance induction in $CD4^+$T cells, where inhibition of the PI3K/Akt pathway enhances $Foxp3^+$Treg induction (Daniel and von Boehmer, 2011; Sauer et al., 2008). Regulation of Foxo transcriptional activity is mainly dependent on the phosphorylation of Foxo proteins via the PI3K/Akt pathway (Daniel and von Boehmer, 2011).

In line with these observations, as one of the more prominently enhanced proteins identified in $CD4^+$T cell proteomes of mice subjected to cold or ADRB3 stimulation, we found C17orf59. It was recently demonstrated to function as a Ragulator-interacting protein that regulates mTORC1 activity through its interaction with Ragulator at the lysosome (Schweitzer et al., 2015). Overexpression of C17orf59 disrupts the Rag-Ragulator complex, prevents Rag lysosomal localization and thereby inhibits mTORC1 activity (Schweitzer et al., 2015). Inhibition of mTORC1 activity, as evidenced by established drugs such as rapamycin or everolimus, directly induces T cell tolerance (Daniel et al., 2010; Sauer et al., 2008; von Boehmer and Daniel, 2013). The increased protein abundance of C17orf59 in $CD4^+$T cells of mice subjected to cold or ADRB3 stimulation supports a concept in which physiological level of ADRB3 stimulation can exert mTORC1-inhibiting activity, thereby directly contributing to the induction of $Foxp3^+$Tregs.

Furthermore, in our unbiased proteomic approach we identified a series of proteins involved in negative regulation of immune responses as well as Treg induction, frequencies and function. Accordingly, we observed regulation of networks that impact Foxp3 itself as well as its interacting partners. Previous analyses indicated that Foxp3 forms large transcriptional complexes comprising several hundred partners (Rudra et al., 2012). Moreover, upon cold exposure or ADRB3 stimulation, we saw upregulation of Foxp3-associated factors implicated in transcription regulation such as Bc11b, CBFβ and Runx1. Some of these Foxp3-bound transcription factors are not only controlled by Foxp3, but also regulate *Foxp3* gene expression by binding to its promoter and intronic enhancers (Rudra et al., 2012). Indeed, targeted ablation of Runx1 or its essential cofactor CBFβ was reported to result in a decreased expression of *Foxp3* mRNA and protein (Kitoh et al., 2009; Rudra et al., 2009).

Recent evidence is emerging that T cell subsets are metabolically distinct (Buck et al., 2016; Chang and Pearce, 2016; Chi, 2012; O'Sullivan and Pearce, 2015), with Tregs being the least glycolytic of the subsets (MacIver et al., 2013). Tregs have elevated rates of lipid oxidation and mitochondrial membrane potentials that are consistent with the observed high level of phosphorylated AMPK. Likewise, AMPK activation, which enhances FAO and energy conservation by antagonizing anabolic pathways, also alters this balance in favor of Tregs (Hardie et al., 2012; Michalek et al., 2011). Accordingly, $CD4^+$T cells from mice subjected to cold exposure or ADRB3 stimulation *in vivo* had higher expression of proteins involved in FAO which can induce Tregs.

In sum, we demonstrate that local $Foxp3^+$Treg induction in adipose tissue involves Stat6/Pten signaling. These findings are consistent with recently emerging hypotheses that local

metabolic changes can link gene regulation, signaling, differentiation and function in order to drive tissue-specific T cell differentiation and fate (Panduro et al., 2016). Moreover, using gain- and loss-of-function studies we demonstrate that Foxp3^{+}Tregs induced by beta-adrenergic signaling or cold exposure are critically required for functional integrity of adipose tissue. Furthermore, we find that local T cell tolerance induction was reduced in the context of impaired BAT-function using UCP1 ablated mice. These findings highlight an important aspect of mutual crosstalk of immune cells and adipocytes in shaping local differentiation programs. Additionally, CD4^{+}T cell proteomes of mice subjected to cold or ADRB3 stimulation identify signatures relevant for Treg induction. Specifically, the Ragulator-interacting protein C17orf59, which limits mTORC1 activity, was upregulated by either ADRB3 stimulation or cold exposure, and therefore might directly enhance Treg induction. In contrast, tolerogenic protein signatures were absent in Stat6ko mice upon ADR3 stimulation *in vivo*. These novel insights into the molecular underpinnings of tissue-specific T cell tolerance induction uncover their role in linking environmental influences with adipose function and metabolic diseases. These discoveries shed new light on potential approaches toward tailored anti-inflammatory concepts to restore metabolic homeostasis in adipose tissue.

STAR Methods

Detailed methods are provided in the online version of this paper and include the following:

Key Resources Table

REAGENT or RESOURCE	SOURCE	IDENTIFIER
Antibodies		
CD4 Biotin	BioLegend	Clone: GK1.5; Cat# 553728; RRID: AB_395012
CD8a Pacific Blue	BioLegend	Clone: 53-6.7; Cat# 100725; RRID: AB_493425
CD11b Pacific Blue	BioLegend	Clone: M1/70; Cat# 101224; RRID: AB_755986
CD11c Brilliant Violett 421	BioLegend	Clone: N418; Cat# 117330; RRID: AB_11219593
B220 Pacific Blue	BioLegend	Clone: RA3-6B2; Cat# 103227; RRID: AB_492876
F4/80 Pacific Blue	BioLegend	Clone: BM8; Cat# 123124; RRID: AB_893475
CD25 PerCP-Cy5.5	BioLegend	Clone: PC61; Cat# 102030; RRID: AB_893288
CD44 PE	BioLegend	Clone: IM7; Cat# 103008; RRID: AB_312959
Ki67 APC	BioLegend	Clone: 16A8; Cat# 652406; RRID: AB_2561930
Ki67 Brilliant Violett 605	BioLegend	Clone: 16A8; Cat# 652413; RRID: AB_2562664
CD4 Alexa Fluor 700	eBioscience	Clone: RM4-5; Cat# 56-0042-82; RRID: AB_494000

REAGENT or RESOURCE	SOURCE	IDENTIFIER
CD62L APC	eBioscience	Clone: MEL-14; Cat# 17-0621-82; RRID: AB_469410
Foxp3 FITC	eBioscience	Clone: FJK-16s; Cat# 11-5773-82; RRID: AB_465243
CD14 V450	BD Biosciences	Clone: rmC5-3; Cat# 560639; RRID: AB_1727429
CD90.1 PerCP-Cy5.5	BioLegend	Clone: OX-7; Cat# 202515; RRID: AB_961438
CD90.2 APC-Cy7	BioLegend	Clone: 30-H12; Cat#105328; RRID: AB_10613293
Anti-mouse CD25 (mCD25)	BioXCell	Clone: PC-61.5.3; Cat# BE0012; RRID: AB_1107619
Fc-Block	BD Pharmingen	Clone: 2.4G2; Cat# 553142; RRID: AB_394657
CD3e	BD Pharmingen	Clone: 145-2C11; Cat# 553057; RRID: AB_394590
CD28	BD Pharmingen	Clone: 37.51; Cat# 553294; RRID: AB_394763
p-Stat6 (pY641) Alexa Fluor 647	BD Phosflow™	Clone: J71-773.58.11; Cat# 558242; RRID: AB_647145
p-Stat6 rabbit anti-mouse	Cell Signaling	Cat# 9361S; RRID: AB_331595
anti-mouse IL-2	eBioscience	Clone: JES6-1A12; Cat# 16-7022-85; RRID: AB_469207
rabbit anti-mouse C17orf59	MyBioSource	polyclonal; Cat# MBS6004199; RRID: N/A
mouse anti-mouse Stat6	Cell Signaling	polyclonal; Cat# 9362; RRID: AB_2271211
rat-anti-mouse LAMP2	BioLegend	Clone: M3/84; Cat# 108502; RRID: AB_313383
Mouse anti-mTOR	Thermo Fisher Scientific	Clone: 215Q18; Cat# AHO1232; RRID: AB_2536329
Hamster anti-mouse CD3	BioLegend	Clone: 145-2C11; Cat# 100302; RRID: AB_312667
Rat anti-mouse CD4	BioLegend	Clone: RM4-5; Cat #100506; RRID: AB_312709
Rat anti-mouse CD4	eBioscience	Clone: GK1.5; Cat# 14-0041-8; RRID: AB_467064
F(ab′)2 donkey anti-rabbit IgG PE	eBioscience	polyclonal; Cat# 12-4739-81; RRID: AB_1210761
goat anti-rat Alexa Fluor 488	Life Technologies	polyclonal; Cat #A11006; RRID: AB_2534074
biotinylated goat-anti-armen. hamster IgG	eBioscience	polyclonal; Cat #13-4113-85; RRID: AB_466651
donkey-anti-mouse AlexaFluor 555	Life Technologies	polyclonal; Cat# A-31570; RRID: AB_2536180
goat-anti-mouse Cy3	Dianova	polyclonal; Cat# 115-165-146; RRID: AB_2491007
goat-anti-rat AlexaFluor 594	Life Technologies	polyclonal; Cat#A11007; RRID: AB_141374
goat anti-rabbit AlexaFluor 594	Life Technologies	polyclonal; Cat# A11012; RRID: AB_141359
rat-anti-mouse biotinylated	Dianova	polyclonal; Cat# 415-065-166; RRID: AB_2340272

REAGENT or RESOURCE	SOURCE	IDENTIFIER
horse anti-rabbit biotinylated	Vector Laboratory	Cat# BA-1100; RRID: AB_2336201
goat-anti-rat STAR580	abberior	Cat# 2-0132-005-1; RRID: N/A
goat-anti-rabbit STAR635P	abberior	Cat# 2-0132-005-5; RRID: N/A
Chemicals, Peptides, and Recombinant Proteins		
Foxp3 Staining Buffer Set	eBioscience	Cat# 00-5523-00
Fixable Viability Dye eFluor450	eBioscience	Cat# 65-0863-18
Sytox Red	Thermo Fisher Scientific	Cat# S34859
Sytox Blue	Thermo Fisher Scientific	Cat# S34857
Streptavidin Microbeads	Miltenyi	Cat #130-048-101
Dynabeads untouched CD4+ mouse	Invitrogen	Cat# 11415D
Streptavidin Alexa Fluor 488	Dianova	Cat# 016-540-084
Streptavidin Dylight 549	Vector Laboratory	Cat# SA-5549
Streptavidin Pacific Blue	Invitrogen	Cat# S11222
Hoechst 33342 dye	Invitrogen	Cat # H1399; CAS 23491-52-3
high fat high sugar (HFHS) diet	Research Diets	Cat# D12331
Pten Inhibitor SF1670	Abcam	Cat# ab141303; CAS 345630-40-2
Stat6 Inhibitor AS 1517499	Axon Medchem	Cat# Axon 1992 ; CAS 919486-40-1
CL-316243	Sigma Aldrich	Cat# C5976; CAS 138908-40-4
cyanopindolol hemifumarate	Tocris	Cat#0993; CAS 69906-86-1
LysC	Wako Chemicals	Cat# 129-02541; EC# 3.4.21.50
trypsin	Sigma Aldrich	Cat# T6567; EC# 232-650-8
ReproSil-Pur C18-AQ 1.9 μm resin	Dr. Maisch GmbH	Cat# R119.b9
Roti-Histofix 4%	Carl Roth	Cat# P087.5
Ficoll-Paque PLUS	GE Healthcare	Cat# 17-1440-03
recombinant human IL-2	ReproTech	Cat# 200-02
collagenase type II	Sigma Aldrich	Cat#C6885; EC #3.4.24.3
collagenase D	Roche	Cat#11088882001; EC #3.4.24.3
Critical Commercial Assays		
miRNeasy Micro Kit	Qiagen	Cat# 217084
Eva Green SuperMix	BioRad	Cat# 1725202
iScript Advanced cDNA Synthesis Kit	BioRad	Cat# 1725038
SMARTer ultra-low input RNA Kit for sequencing – v4	Takara Clonetech	Cat# 634890
SMARTer Universal Low Input RNA Kit for Sequencing	Takara Clonetech	Cat# 634889
Deposited Data		
mass spectrometry data	This paper	ProteomeXchange Consortium via PRIDE repository; Identifier: ProteomeXchange: PXD004671
Experimental Models: Organisms/Strains		

REAGENT or RESOURCE	SOURCE	IDENTIFIER
CD90.1 Balb/c; genotype: CBy.PL(B6)-*Thy1*^{a}/ScrJ	Jackson Laboratory	RRID: IMSR_JAX:005443
CD90.2 Balb/c; genotype: Balb/cByJ	Jackson Laboratory	RRID: IMSR_JAX:001026
Foxp3 GFP Balbc; genotype: C.Cg-Foxp3^{tm2Tch}/J	Jackson Laboratory	RRID: IMSR_JAX:006769
Foxp3 GFP Bl6; genotype: B6.Cg-Foxp3^{tm2Tch}/J	Jackson Laboratory	RRID: IMSR_JAX:006772
Stat6VT+ Bl6; genotype: Stat6 VT/AA mutation	Mark H. Kaplan, Indiana University, USA (Bruns et al., 2003)	N/A
Stat6KO Balbc; genotype: C.129S2-*Stat6*^{tm1Gru}/J	Mark H. Kaplan, Indiana University, USA (Kaplan et al., 1996)	RRID: IMSR_JAX:002828
Stat6KO 4get-GFP, Balbc	Benno Weigmann, University Erlangen, Germany (Gessner et al., 2005)	N/A
PtenTg Bl6	Manuel Serrano, Spanish National Cancer Research Center, Spain (Ortega-Molina et al., 2012)	N/A
Betaless; genotype: Adrb1,2,3TKO	Francoise Rohner-Jeanrenaud, University of Geneva, Switzerland	N/A
Borcs6$^{+/-}$; genotype: B6N(Cg)-*Borcs6*$^{tm1.1(KOMP)Vlcg}$/J	Jackson Laboratory	RRID: IMSR_JAX:028178
Humanized mice; genotype: *NOD.Cg-Prkdc*^{scid}*H2-Ab1*^{tm1Gru}*Il2rg*^{tm1Wjl}Tg(HLA-DQA1,HLA-DQB1)1Dv//Sz	Leonard Shultz, Jackson Laboratory	N/A
Foxp3-DTR; genotype: C57BL/6-Tg(Foxp3-DTR/EGFP)23.2Spar/Mmjax	Tobias Bopp, Johannes Gutenberg University Mainz, Germany	RRID: MMRRC_032050-JAX
Sequence-Based Reagents		
Custom primers used for qPCR	This paper	Table S1
Software and Algorithms		
FlowJo software (version 7.6.1)	TreeStar, OR	https://www.flowjo.com/solutions/flowjo/dow
FACSDiva software (version 6.1.3)	Beckton Dickinson	N/A
Prism (version 6.0.1)	GraphPad	https://www.graphpad.com/scientific-software
Statistical Package for the Social Sciences (SPSS) (version 19.0)	IBM	https://www-01.ibm.com/software/de/analytics
SprayQc software	(Scheltema and Mann, 2012)	http://sprayqc.sourceforge.net/
MaxQuant software package (version 1.5.3.29)	(Cox and Mann, 2008)	http://www.coxdocs.org/doku.php?id=maxqua
Andromeda search engine	(Cox et al., 2011)	http://www.coxdocs.org/doku.php?id=maxqua
iBAQ algorithm	(Schwanhäusser et al., 2011)	N/A
Perseus software package	(Tyanova, 2016)	http://www.coxdocs.org/doku.php?id=perseus
DESeq2	(Love et al., 2014)	https://bioconductor.org/packages/release/bioc
SAMTools	(Li et al., 2009)	N/A
FastQC	(Andrews, 2010)	http://www.bioinformatics.babraham.ac.uk/pro
HTSeq-count	(Anders et al., 2015)	http://www-huber.embl.de/users/anders/HTSe

Contact for reagent sharing

Further information and requests for resources and reagents should be directed to and will be fulfilled by Matthias Tschoep (Tschoep@helmholtz-muenchen.de)

Experimental model and subject details

Mice—CBy.PL(B6)-*Thy1*^{a}/ScrJ (CD90.1 Balbc), Balb/cByJ (CD90.2 Balbc), C.Cg-Foxp3^{tm2Tch}/J (Foxp3 GFP Balbc) and B6.Cg-Foxp3^{tm2Tch}/J mice (Foxp3 GFP Bl6) mice were originally obtained from Jackson Laboratories. C.129S2-*Stat6*^{tm1Gru}/J (Kaplan et al., 1996), referred to as Stat6ko mice, and Stat6VT mice (Bruns et al., 2003) were previously described. Pten Tg Bl6 mice were kindly provided by Manuel Serrano (Spanish National Cancer Research Center (CNIO), Spain). Adrb1,2,3TKO mice, referred to as betaless mice, were kindly provided by Francoise Rohner-Jeanrenaud (Faculty of Medicine, University of Geneva, Switzerland). Humanized mice, *NOD.Cg-Prkdc*^{scid} *H2-Ab1*^{tm1Gru} *Il2rg*^{tm1Wjl} Tg(HLA-DQA1,HLA-DQB1)1Dv//Sz mice, lack murine MHC class II and transgenically express human HLA-DQ8. These mice were developed by Leonard Shultz at the Jackson Laboratory. For high-caloric challenge, mice were fed *ad libitum* with a high-fat, high-sugar (HFHS) diet composed of 58.0% kcal from fat, 25.5% kcal from carbohydrates (including 8% sucrose) and 16.4% kcal from protein (Research Diets, #D12331, New Brunswick, NJ) or standard diet (Altromin, #1314, Lage, Germany) for 1–16 wk. Mice were maintained group-housed on a 12h/12h light dark cycle at 25°C under specific pathogen free (SPF) conditions. All mice had *ad libitum* access to food and water and were maintained in the animal facility of the Helmholtz Zentrum München, Munich, Germany according to guidelines established by the Institutional Animal Committees. C57BL/6-Tg(Foxp3-DTR/EGFP)23.2Spar/Mmjax mice, referred to as Foxp3 DTR mice, were kindly provided by Tobias Bopp (Institute of Immunology, University Medical Center Mainz, Johannes Gutenberg-University, Mainz, Germany) and Stat6KO 4get-GFP Balbc mice (Gessner et al., 2005) were kindly provided by Benno Weigmann (Department of Medicine 1, University of Erlangen-Nuremberg, Erlangen, Germany). These mice were maintained at the animal facility of the I. Medical Clinic, University of Erlangen-Nuremberg, Erlangen, Germany. Mice were randomized to test groups. For *in vivo* ADRB3 stimulation or inhibition mice were injected *i.p.* with 1 mg/kg CL or 0.3 mg/kg Cyanopindolol on three consecutive days, respectively. 0.9% NaCl was used as vehicle control. For Treg depletion, Foxp3 DTR mice were injected *i.p.* with 50 ng diphtheria toxin per g bodyweight on three consecutive days. As second approach of Treg depletion, 250 μg anti-mCD25 antibodies (BioXCell) were injected *i.p.* on three consecutive days (Setiady et al., 2010). For *in vivo* Treg expansion, 6 μg anti-IL2/IL2 antibody (IL-2-mAb) complexes were injected *s.c.* on three consecutive days (Webster et al., 2009). For *in vivo* cold exposure experiments, mice were acclimated to 8°C for 1 wk or to 4°C for 24 h as indicated in the text. No animals were excluded due to illness or outlier results; therefore, no exclusion determination was required. The investigators were not blinded to group allocation or to the assessment of experimental end points. All animal care was executed according to guidelines established by the Institutional Animal Committees at each institution. Ethical approval for all mouse experimentations has been received by corresponding local animal welfare authorities (District government of upper Bavaria or Veterinary office of Zurich).

Human subjects and samples—Venous blood was collected from healthy adults (n=2, female, age 25) who consented to the *Munich Bioresource project (approval number #5049/11, Technische Universität München, Munich, Germany)* in heparinized blood collection tubes (BD Vacutainer Blood Collection Tubes, Becton Dickinson). For human adipose tissue samples, paired samples of abdominal subcutaneous (scWAT) and omental whole adipose tissue (visWAT) were obtained from individuals, which were lean (n=6, mean BMI: 23.2kg/m^2). Phenotypic characterization of the study participants was performed as previously described (Kloting et al., 2010). All adipose tissue samples were collected during open or laparoscopic abdominal surgery as described previously (Kloting et al., 2010). The study was approved by the Ethics Committee of the University of Leipzig (*approval number #159-12-21052012* and #*017-12-23012012*) and performed in accordance to the declaration of Helsinki. All subjects gave written informed consent before taking part in a study.

***In vitro* studies with primary murine T cells—**Freshly isolated murine $CD4^+$ T cells were cultured for three days in RPMI media (Gibco by life technologies™) supplemented with 10% FCS, 1 mM sodium pyruvate (Sigma Aldrich), 50 mM β-mercaptoethanol (Amimed), 1X non-essential amino acids (Merck Millipore), 100 U/ml human recombinant IL-2 (ReproTech), 100 U/ml penicillin and 100 μg/ml streptomycin (Sigma Aldrich) at 37°C in an humidified CO_2 incubator. Cell culture treated 96 well U bottom plates were used (Bio-Greiner one).

***In vitro* studies with primary human T cells—**Freshly isolated human $CD4^+$ T cells were cultured in Vivo15 Medium supplemented with 2 mM glutamine, penicillin (50 U/ml) (Sigma Aldrich), streptomycin (50 μg/ml) (Sigma Aldrich), 100 U/ml human recombinant IL-2 (ReproTech) and 5% (vol/vol) heat-inactivated human AB serum (Invitrogen) in 96-well U bottom plates (Bio-Greiner one). in an humidified CO_2 incubator.

Method Details

Isolation of $CD4^+$T cells from lymphoid organs—Lymph nodes and spleens were mashed through 70 μm cell strainers in $HBSS^+$ (supplemented with 5% FCS and 10 mM HEPES). After surface antibody staining, $CD4^+$T cells were enriched using biotin-labelled anti-CD4 antibodies and magnetic activated cell sorting (MACS, Miltenyi) with streptavidin microbeads (Miltenyi). Streptavidin-fluorochrome-conjugates (molecular probes by life technologies) were added after 5 min to allow flow cytometric detection. Cells were further processed for FACS sorting as described below. For immunofluorescence experiments, T cells were isolated from lymph nodes using Dynabeads® untouched™ Mouse CD4 Kit (Invitrogen) according to manufacturer's instructions.

Isolation of $CD4^+$T cells from adipose tissues—*White adipose tissue* was collected in PBS supplemented with 0.5% BSA and digested with Collagenase II solution [3–4 mg/ml Collagenase II, 10 mM $CaCl_2$] for 10 minutes at 37°C on a rotator. The cell suspension was passed through a 200 μm nylon mesh and centrifuged (380xg, 5 min., 4°C) to separate the stromal vascular fraction from adipocytes. Pelleted cells were re-suspended in $HBSS^+$ (HBSS supplemented with 5% FCS and 10 mM HEPES) and stained for flow cytometric analysis. *Brown adipose tissue* was digested in three digestion rounds with 1 mg/ml

Collagenase D in HBSS$^+$ at 37°C for 20 min on a rotator. Cell suspensions were passed through a 200 μm nylon mesh and stained for flow cytometric analysis.

Human cell isolation from blood—Peripheral blood mononuclear cells (PBMC) were isolated by density centrifugation over Ficoll-Paque PLUS (GE Healthcare). Human CD4$^+$T cells were isolated from fresh PBMCs via MACS enrichment with CD4$^+$ microbeads following the manufacturer's protocol.

Cell staining for flow cytometry

Murine FACS stainings: The following monoclonal antibodies were used for **murine FACS stainings**: From BioLegend (San Diego, CA): anti-CD4 Biotin (GK1.5, 1:400), anti-CD8a Pacific Blue (53-6.7; 1:300), anti-CD11b Pacific Blue (M1/70, 1:300), anti-CD11c Brilliant Violett 421 (N418, 1:400), anti-B220 Pacific Blue (RA3-6B2, 1:300), anti-F4/80 Pacific Blue (BM8, 1:400), anti-CD25 PerCP-Cy5.5 (PC61, 1:200), anti-CD44 PE (IM7, 1:800, 1:3000 for analysis with ≤1,000 cells per well), anti-Ki67 APC (16A8, 1:400); anti-Ki67 Brilliant Violett 605 (16A8, 1:400), anti-CD90.1 PerCP-Cy5.5 (OX-7, 1:500), anti-CD90.2 APC-Cy7 (30-H12, 1:500); from eBioscience (San Diego, CA): anti-CD4 Alexa Fluor 700 (RM4-5; 1:200; 1:600 for analysis with ≤1,000 cells), anti-CD62L APC (MEL-14, 1:400), anti-Foxp3 FITC (FJK-16s, 1:200), polyclonal donkey anti-rabbit IgG PE (1:2000); from BD Biosciences: anti-CD14 V450 (rmC5-3, 1:400). Unspecific binding of antibodies was prevented by incubation of cell suspensions with Fc-Block (BD Pharmingen, 2.4G2, 1:100) for 10 min on ice, followed by flow cytometric staining for 30 min on ice in the dark. Cells were passed through a 40 μm cell strainer (NeoLab) to remove large debris. Enumeration of cells and acquisition were performed by using FACSAriaIII and FACSDiva software (BD version 6.1.3). Single-cell data analyses were performed by the use of the FlowJo software 7.6.1 (Tree Star Inc., OR).

Human FACS stainings: The following monoclonal antibodies were used for human FACS stainings: from BD Biosciences (San Jose, CA): anti-CD25 APC (2A3, 1:20), anti-CD45RO APC-H7 (UCHL1, 1:20), anti-CD4 V500 (RPA-T4, 1:20); from Biolegend (San Diego, CA): anti-CD45RA FITC (HI100, 1:20), anti-CD3 PerCP-Cy5.5 (HIT3a, 1:20), anti-CD127 PE-Cy7 (A019D5, 1:20), anti-CD8a Pacific Blue (RPA-T8, 1:50), anti-CD11b Pacific Blue (ICRF44, 1:50), anti-CD14 Pacific Blue (HCD14, 1:50), anti-CD19 Pacific Blue, anti-CD3 Alexa Fluor 700 (HIT3a, 1:20), anti-CD45 Alexa Fluor 700 (HI30, 1:20), anti-Ki67 APC (16A8, 1:200) or anti-Ki67 Brilliant Violet 605 (16A8, 1:400); from eBioscience (San Diego, CA): anti-Foxp3 Alexa Fluor 700 (PCH101, 1:100), anti-Foxp3 PE (236A/E7, 1:100); Unspecific binding of antibodies was prevented by incubation of cell suspensions with Fc-Block (Human TruStain FcX, BioLegend, 1:20) for 5 min at RT, followed by FACS staining for 20 min at RT in the dark. Cells were passed through a 40 μm cell strainer (NeoLab) to remove large debris.

Intracellular staining: To detect intracellular protein expression, T cells were fixed and permeabilized using the Foxp3 Staining Buffer Set (eBioscience) after surface staining. For phospho-Stat6 stainings, MACS-enriched CD4$^+$ T cells were cultured over night with 5 μg/ml plate-bound anti-CD3 and anti-CD28 in RPMI media with supplements and 100 U/ml

IL-2. Cells were washed and re-stimulated with CL (100 nM) for 15 min. Surface staining was performed as described above with Fc Block supplemented with sodium vanadate (New England Biolabs). Cells were fixed with PFA (4.5% Histofix, Carl Roth) and permeabilized with 100% methanol. Anti-phospho Stat6-AlexaFluor 647 was stained as recommended by the manufacturer.

Sample acquisition: Cells were acquired on BD FACSAriaIII flow cytometer using FACSDiva software with optimal compensation and gain settings determined for each experiment based on unstained and single-color stained samples. Doublets were excluded based on SSC-A vs. SSC-W plots and FSC-A vs. FSC-W plots. Live cell populations were gated on the basis of cell side and forward scatter and the exclusion of cells positive for Sytox Blue (Life Technologies) or Fixable Viability Dye eFluor450 (eBioscience). Samples were analyzed using FlowJo software version 7.6.1 (TreeStar Inc., OR).

Analysis of mitochondrial membrane potentials—The analysis of mitochondrial membrane potentials of $CD4^+$T cells was performed on FACS sort-purified $CD4^+$T cells from lymphoid organs and adipose tissues with BD™ MitoScreen Kit (BD) according to the manufacturer's instructions. T cells incubated with 250 μM H_2O_2 for 2 hours at 37°C prior to staining with JC-1 dye were used as positive controls, while unstained cells were used as negative control. Analysis was performed on the FACSAriaIII (BD) flow cytometer.

***In vitro* Treg-induction assay—**Murine naïve $CD4^+$T cells were defined as $CD4^+CD25^-Foxp3^-GFP^-CD44^{low}$ for Foxp3-GFP reporter mice and as $CD4^+CD25^-CD44^{low}$ for non-reporter mice. Cells were sorted with a FACSAriaIII (BD) cell sorter for purity. Murine naïve $CD4^+$T cells were cultured for 18 hours in RPMI media (Gibco by life technologies™) supplemented with 10% FCS, 1 mM sodium pyruvate (Sigma Aldrich), 50 mM β-mercaptoethanol (Amimed), 1X non-essential amino acids (Merck Millipore), 100 U/ml human recombinant IL-2 (ReproTech), 100 U/ml penicillin and 100 μg/ml streptomycin (Sigma Aldrich), while human naïve $CD3^+CD4^+CD45RA^+CD45RO^-CD127^+CD25^-$ T cells were cultured in Vivo15 Medium supplemented with 2 mM glutamine, penicillin (50 U/ml), streptomycin (50 μg/ml), and 5% (vol/vol) heat-inactivated human AB serum (Invitrogen) in 96-well plates pre-coated with 5 μg/ml anti-CD3e (145-2C11, BD Pharmingen) and 5 μg/ml anti-CD28 (37.51, BD Pharmingen). TCR stimulation was limited to 18 hours by transferring cells into uncoated wells. Cells were cultured for additional 36 hours without further TCR stimulation.

Chemicals and enzymes used for experiments—To test the influence of adrenergic receptor stimulation or inhibition on Treg induction capacities, chemicals were added to *in vitro* cultures in the concentrations given in the text: CL-316243 (Sigma Aldrich, CAS 138908-40-4), Cyanopindolol hemifumarate (Tocris, CAS 69906-86-1) and Mirabegron (Selleckchem, CAS 223673-61-8). To evaluate the influence of specific signaling pathways on Treg induction we used a specific PTEN inhibitor SF1670 (Abcam, CAS 345630-40-2) and a specific Stat6 inhibitor AS 1517499 (Axon Medchem, CAS 919486-40-1). Collagenase type II (Sigma Aldrich, EC #3.4.24.3) and Collagenase D (Roche, EC #3.4.24.3) were used for T cell isolation from adipose tissues.

Quantitative analysis of mRNA abundance

RNA extraction and cDNA synthesis: Total RNA was extracted from sort-purified T cell populations using QIAzol Lysis Reagent/ miRNeasy Micro Kit and from snap-frozen total tissue samples (BAT, scWAT, visWAT), which were previously homogenized using QIAshredder (Qiagen) according to the manufacturer's instructions. 1 µg total RNA was converted to first strand cDNA using iScript™ Advanced cDNA Synthesis Kit (Bio-Rad). For cell numbers < 2000 and/or RNA amounts < 200 ng, cDNA synthesis and subsequent amplification was performed using the SMARTer ultra-low input RNA Kit for sequencing – v4 or SMARTer Universal Low Input RNA Kit for Sequencing (Takara Clonetech) according to the manufacturer's instructions. cDNA was generated in the Thermal Cycler peqStar 2X (Peqlab). Real-time PCR quantification was performed using SsoFast Evagreen Supermix (Bio-Rad) or SYBR® Premix Ex Taq™ (Takara Clonetech) and gene-specific primer sets on a CFX96 real time system (Bio-Rad). *Histone* and *18S* RNA levels were used for normalization of target gene expression levels. Analysis of candidate genes involved in thermogenesis, browning, lipolysis, glycolysis and inflammation was performed. *Primers* used for Quantitative Real-Time PCR analyses are listed in Supplemental Table S1.

Gel electrophoresis: 2% (w/v) peqGOLD Universal Agarose (Peqlab) was dissolved in 1X TAE Buffer (Applichem) and 3 µL/100 mL Midori Green Advance (Biozym Scientific) were added. Products from RT-qPCR were mixed with Gel Loading Dye Blue (BioLabs). 100 bp Ladder (New England Biolabs) was used as reference. Gel electrophoresis was performed with 130 V for 40–120 min using the power supply unit peqPOWER E250 (Peqlab). DNA fragments were detected using FUSION-FX7 Spectra (Vilber).

mRNA expression profiling: cDNA Synthesis: cDNA was generated directly from cells in the Thermal Cycler peqStar 2X (Peqlab) using the SMARTer ultra-low input RNA Kit for sequencing – v4 or SMARTer Universal Low Input RNA Kit for Sequencing (Takara Clonetech) according to the manufacturer's instructions. mRNA expression profiling using next generation sequencing (NGS). For NGS, cDNA concentration and integrity (quality) of the samples were assessed using Agilent High Sensitivity DNA Chips (Agilent Technologies) and Agilent 2100 Bioanalyzer. We employed NGS for expression profiling in pooled sample-sets of $CD4^+$T cells purified from white and brown fat. mRNA library preparation was conducted with Nextera reagents (Illumina), according to the manufacturer's instructions. NGS was performed on a NextSeq (Illumina) with 75bp single end reads for mRNA using Illumina reagents and following the manufacturer's instructions.

NGS data processing and statistical analysis: Quality was assessed by FastQC (Andrews, 2010). Reads were mapped to the mouse genome (mm10) using BWA-mem with default configuration. Read counts lists were created using SAMTools (Li et al., 2009) and HTSeq-count (Anders et al., 2015). Reads were normalized using DESeq2 (Love et al., 2014). Normalized read counts were further processed for descriptive visualization of expression trends for this preliminary experiment. The cut-off for reading counts was set to 30 and pseudogenes were manually removed. The top 5 upregulated genes are shown.

Proteomics—Mice were treated for three days with 1 mg/kg CL316243 or 0.9% NaCl as vehicle control *in vivo*. Additionally, mice were subjected to cold exposure (8°C) vs. room temperature for 1 week $CD4^+$T cells were isolated by MACS enrichment using CD4-biotin antibodies and streptavidin microbeads as described above.

Sample preparation for LC-MS/MS analysis: Cell lysis of isolated cells was performed in LB buffer (50% (v/v) 2-2-2-trifluoroethanol (TFE) plus 2 mM dithiothreitol, 50% (v/v) 50 mM ammonium bicarbonate (ABC) buffer) at 99°C for 10 min followed by sonication for 10 min (10 cycles high intensity, Bioruptor, Diagenode). Cell debris was removed after 10 min centrifugation (16,000 g at 4°C) and proteins in the lysate were alkylated for 30 min with 10 mM iodoacetamide in the dark. Next, the solution was centrifuged in a vacuum evaporator for about three hours at 45°C. Proteins were resolubilized in 10% (v/v) TFE in 50 mM ABC and sonicated in a water bath for 5 min. Proteins were digested by adding 0.2 μg of LysC and 0.2 μg of Trypsin and incubation at 37°C overnight. The next day, the digest was stopped by adding 1% (v/v) TFE and the solution volume was reduced in a vacuum evaporator for about one hour at 45°C. Samples were finally desalted on SDB-RPS StageTips (3M, Empore, Neuss, Germany) and eluted as described (Kulak et al., 2014).

LC-MS/MS analysis: MS analysis was performed using Q-Exactive HF mass spectrometers (Thermo Fisher Scientific, Bremen, Germany) coupled on-line to a nanoflow UHPLC instrument (Easy nLC, Thermo Fisher Scientific). Peptides were separated on a 50 cm long (75 μm inner diameter) column packed in-house with ReproSil-Pur C18-AQ 1.9 μm resin (Dr. Maisch GmbH, Ammerbuch, Germany). Column temperature was kept at 50 °C by an in-house designed oven with a Peltier element and operational parameters were monitored in real time by the SprayQc software (Scheltema and Mann, 2012). Peptides were loaded with buffer A (0.1% (v/v) formic acid) and eluted with a nonlinear gradient of 5–60% buffer B (0.1% (v/v) formic acid, 80% (v/v) acetonitrile) at a flow rate of 300 nl/min. Peptide separation was achieved by 120 min gradients. The survey scans (300–1650 m/z, target value = 3E6, maximum ion injection times = 20ms) were acquired at a resolution of 60,000 followed by higher-energy collisional dissociation (HCD) based fragmentation (normalized collision energy = 27) of up to 15 dynamically chosen, most abundant precursor ions (isolation window = 1.4 m/z). The MS/MS scans were acquired at a resolution of 15,000 (target value = 1E5, maximum ion injection times = 60 ms). Repeated sequencing of peptides was minimized by excluding the selected peptide candidates for 20 s.

Computational MS data analysis: All data was analyzed using the MaxQuant software package 1.5.3.29 (Cox and Mann, 2008). The false discovery rate (FDR) cut-off was set to 1% for protein and peptide spectrum matches. Peptides were required to have a minimum length of 7 amino acids and a maximum mass of 4600 Da. MaxQuant was used to score fragmentation scans for identification based on a search with an initial allowed mass deviation of the precursor ion of a maximum of 4.5 ppm after time-dependent mass calibration. The allowed fragment mass deviation was 20 ppm. Fragmentation spectra were identified using the UniprotKB *Mus musculus* database (UniProt, 2015), based on the 2014_07 release, combined with 262 common contaminants by the integrated Andromeda search engine (Cox et al., 2011). Enzyme specificity was set as C-terminal to arginine and

lysine, also allowing cleavage before proline, and a maximum of two missed cleavages. Carbamidomethylation of cysteine was set as fixed modification and N-terminal protein acetylation as well as methionine oxidation as variable modifications. Both 'label-free quantification (MaxLFQ)' and 'match between runs' with standard settings were enabled (Cox et al., 2014). Protein copy number estimates were calculated using the iBAQ algorithm (Schwanhäusser et al., 2011).

Statistics and Data visualization

Basic data handling, normalization, statistics and annotation enrichment analysis was performed with the Perseus software package (Tyanova, 2016). We filtered for protein groups that were quantified with at least two valid values in at least one group of triplicates. Missing values were imputed with values representing a normal distribution (generated at 1.8 standard deviations of the total intensity distribution, subtracted from the mean, and a width of 0.3 standard deviations). Differentially expressed proteins were identified by one-way ANOVA test at a permutation-based FDR cutoff of 0.05. Enrichment for annotation categories was evaluated by 1D annotation enrichment or Fisher exact test to obtain a p-value. The mass spectrometry proteomics data have been deposited to the ProteomeXchange Consortium (Vizcaino et al., 2014) via the PRIDE partner repository with the dataset identifier PXD004671.

Immunefluorescence by confocal microscopy—T cells were isolated from thymus and lymph nodes with Dynabeads untouched $CD4^+$ mouse kit (Invitrogen) according to the manufacturer's instructions. Isolated cells were fixed with PFA (Histofix 4.5%, Carl Roth) for 10 min at RT. Immunofluorescence staining was done using rat-anti-mCD4 antibodies (RM4-5; BioLegend) and goat-anti-rat antibodies conjugated with AlexaFluor488 dye (Life Technologies). For CD3 staining armenian hamster-anti-mouse antibodies (145-2C11; BioLegend) were used together with biotinylated goat-anti-hamster antibodies followed by streptavidin-AlexaFluor488 (Life Technologies). For mTOR immunofluorescence analyses, mouse-anti-mTOR antibodies (215Q18; Thermo) and donkey-anti-mouse antibodies conjugated with AlexaFluor555 (Life Technologies) were used. For CD107b staining rat-anti-mouse LAMP2 (M3/84; BioLegend) antibodies were used followed by goat-anti-rat antibodies conjugated with AlexaFluor488 dye (Life Technologies). STAT6 was stained using mouse-anti-mSTAT6 antibodies followed by goat-anti-mouse antibodies conjugated with Cy3 dye. Negative control slides were incubated with secondary antibodies only. In most experiments the cells were PFA-fixed and prepared with cytospin centrifuge (Shandon). For Foxp3 staining, T cells were aceton-fixed, incubated with rat-anti-mouse antibodies (eBioscience) and goat-anti-rat antibodies conjugated with AlexaFluor594 dye (BioLegend). Nuclei were counterstained with DAPI (Vector). Finally, cells were analyzed by confocal microscopy (Leica DMI6000CS).

Immunefluorescence by STED microscopy—Untouched $CD4^+$T cells from inguinal lymph nodes were fixed with PFA for 10 min at RT. After permeabilization with TritonX100 for 5 min and protein block for 10 min with 2% BSA, staining of rat anti-CD4 antibody (BD) and rabbit anti-C17orf59 antibody (MyBioSource) was performed. Goat-anti-rat-STAR580 (abberior) and goat-anti-rabbit STAR635P (abberior) were used as secondary

antibodies. Finally, nuclei were counterstained with DAPI. Negative control slides were incubated with secondary antibodies only. Cells were analyzed by Abberior 3D STED 2-Channel Super Resolution Microscope (Abberior, Göttingen). The dye STAR580 was excited with a 594 nm pulsed laser, STAR635p with a 640 nm pulsed laser and DAPI with a 405 nm CW laser and depletion of STAR580 + STAR635p was done with a 775 nm pulsed STED laser.

Quantification and statistical analysis

Results are presented as means±SEM, as percentage, where appropriate or as summary box-and-whisker plots indicating minimum to maximum values to demonstrate data distribution. For normally distributed data, Student's t-test for unpaired values was used to compare independent groups. Group size estimations were based upon a power calculation to minimally yield an 80% chance to detect a significant difference in the respective parameter of $P< 0.05$ between the relevant groups. For all tests, a two-tailed p value of <0.05 was considered to be significant. Statistical significance is shown as * = $P<0.05$; ** = $P<0.01$; *** = $P<0.001$. N numbers can be found within the text and/or within the figure legends. Analyses were performed using GraphPad Prism 6.0.1 (La Jolla, CA) and the Statistical Package for the Social Sciences (SPSS 19.0; SPSS Inc., Chicago, IL).

Data and software availability

Data resources—The mass spectrometry proteomics data have been deposited to the ProteomeXchange Consortium (Vizcaino et al., 2014) via the PRIDE partner repository with the dataset identifier PXD004671.

Supplementary Material

Refer to Web version on PubMed Central for supplementary material.

Acknowledgments

The authors thank Siegfried Ussar for helpful discussions, Michael Pfaffl and the EMBL Genecore facility and its personnel, especially Vladimir Benes, for providing reagents, materials and analysis tools for next generation sequencing. CD is supported by a Research Group at Helmholtz Zentrum München and the German Center for Diabetes Research (DZD) and received support through a membership in the CRC1054 of the Deutsche Forschungsgemeinschaft (B11). MHK is supported by a Public Health Services award (AI095282). BW is supported by WE 4656/2 and DFG-CRC1811 (B02). MHT is supported by the Alexander von Humboldt Foundation, the DZD, and the Helmholtz Alliance ICEMED-Imaging and Curing Environmental Metabolic Diseases, through the Initiative and Networking Fund of the Helmholtz Association.

References

Anders S, Pyl PT, Huber W. HTSeq--a Python framework to work with high-throughput sequencing data. Bioinformatics. 2015; 31:166–169. [PubMed: 25260700]

Andrews, S. FastQC: a quality control tool for high throughput sequence data. 2010. Available online at: http://www.bioinformatics.babraham.ac.uk/projects/fastqc

Bachman ES, Dhillon H, Zhang CY, Cinti S, Bianco AC, Kobilka BK, Lowell BB. βAR Signaling Required for Diet-Induced Thermogenesis and Obesity Resistance. Science. 2002; 297:843–845. [PubMed: 12161655]

Bapat SP, Myoung Suh J, Fang S, Liu S, Zhang Y, Cheng A, Zhou C, Liang Y, LeBlanc M, Liddle C, et al. Depletion of fat-resident Treg cells prevents age-associated insulin resistance. Nature. 2015; 528:137–141. [PubMed: 26580014]

Bruns HA, Schindler U, Kaplan MH. Expression of a Constitutively Active Stat6 In Vivo Alters Lymphocyte Homeostasis with Distinct Effects in T and B Cells. The Journal of Immunology. 2003; 170:3478–3487. [PubMed: 12646608]

Buck MD, O'Sullivan D, Klein Geltink RI, Curtis JD, Chang CH, Sanin DE, Qiu J, Kretz O, Braas D, van der Windt GJ, et al. Mitochondrial Dynamics Controls T Cell Fate through Metabolic Programming. Cell. 2016; 166:63–76. [PubMed: 27293185]

Chang CH, Pearce EL. Emerging concepts of T cell metabolism as a target of immunotherapy. Nat Immunol. 2016; 17:364–368. [PubMed: 27002844]

Chapoval S, Dasgupta P, Dorsey NJ, Keegan AD. Regulation of the T helper cell type 2 (Th2)/T regulatory cell (Treg) balance by IL-4 and STAT6. Journal of Leukocyte Biology. 2010; 87:1011–1018. [PubMed: 20335310]

Chi H. Regulation and function of mTOR signalling in T cell fate decisions. Nat Rev Immunol. 2012; 12:325. [PubMed: 22517423]

Cipolletta D, Cohen P, Spiegelman BM, Benoist C, Mathis D. Appearance and disappearance of the mRNA signature characteristic of Treg cells in visceral adipose tissue: age, diet, and PPARgamma effects. Proc Natl Acad Sci U S A. 2015; 112:482–487. [PubMed: 25550516]

Cipolletta D, Feuerer M, Li A, Kamei N, Lee J, Shoelson SE, Benoist C, Mathis D. PPAR-gamma is a major driver of the accumulation and phenotype of adipose tissue Treg cells. Nature. 2012; 486:549–553. [PubMed: 22722857]

Cox J, Hein MY, Luber CA, Paron I, Nagaraj N, Mann M. Accurate proteome-wide label-free quantification by delayed normalization and maximal peptide ratio extraction, termed MaxLFQ. Molecular & cellular proteomics : MCP. 2014; 13:2513–2526. [PubMed: 24942700]

Cox J, Mann M. MaxQuant enables high peptide identification rates, individualized p.p.b.-range mass accuracies and proteome-wide protein quantification. Nat Biotechnol. 2008; 26:1367–1372. [PubMed: 19029910]

Cox J, Neuhauser N, Michalski A, Scheltema RA, Olsen JV, Mann M. Andromeda: a peptide search engine integrated into the MaxQuant environment. Journal of proteome research. 2011; 10:1794–1805. [PubMed: 21254760]

Cypess AM, Weiner LS, Roberts-Toler C, Franquet Elia E, Kessler SH, Kahn PA, English J, Chatman K, Trauger SA, Doria A, et al. Activation of human brown adipose tissue by a beta3-adrenergic receptor agonist. Cell Metab. 2015; 21:33–38. [PubMed: 25565203]

Cypess AM, White AP, Vernochet C, Schulz TJ, Xue R, Sass CA, Huang TL, Roberts-Toler C, Weiner LS, Sze C, et al. Anatomical localization, gene expression profiling and functional characterization of adult human neck brown fat. Nature Medicine. 2013; 19:635–639.

Daniel C, von Boehmer H. Extrathymic generation of regulatory T cells--chances and challenges for prevention of autoimmune disease. Adv Immunol. 2011; 112:177–213. [PubMed: 22118409]

Daniel C, Weigmann B, Bronson R, Boehmer Hv. Prevention of type 1 diabetes in mice by tolerogenic vaccination with a strong agonist insulin mimetope. J Exp Med. 2011; 208:1501–1510. [PubMed: 21690251]

Daniel C, Wennhold K, Kim HJ, von Boehmer H. Enhancement of antigen-specific Treg vaccination in vivo. Proc Natl Acad Sci U S A. 2010; 107:16246–16251. [PubMed: 20805478]

Fedorenko A, Lishko PV, Kirichok Y. Mechanism of fatty-acid-dependent UCP1 uncoupling in brown fat mitochondria. Cell. 2012; 151:400–413. [PubMed: 23063128]

Feldmann HM, Golozoubova V, Cannon B, Nedergaard J. UCP1 ablation induces obesity and abolishes diet-induced thermogenesis in mice exempt from thermal stress by living at thermoneutrality. Cell Metab. 2009; 9:203–209. [PubMed: 19187776]

Feuerer M, Herrero L, Cipolletta D, Naaz A, Wong J, Nayer A, Lee J, Goldfine AB, Benoist C, Shoelson S, et al. Lean, but not obese, fat is enriched for a unique population of regulatory T cells that affect metabolic parameters. Nat Med. 2009; 15:930–939. [PubMed: 19633656]

Gessner A, Mohrs K, Mohrs M. Mast Cells, Basophils, and Eosinophils Acquire Constitutive IL-4 and IL-13 Transcripts during Lineage Differentiation That Are Sufficient for Rapid Cytokine Production. The Journal of Immunology. 2005; 174:1063–1072. [PubMed: 15634931]

Goenka S, Kaplan MH. Transcriptional regulation by STAT6. Immunologic research. 2011; 50:87–96. [PubMed: 21442426]

Gottschalk RA, Corse E, Allison JP. TCR ligand density and affinity determine peripheral induction of Foxp3 in vivo. J Exp Med. 2010; 207:1701–1711. [PubMed: 20660617]

Guillot X, Tordi N, Mourot L, Demougeot C, Dugue B, Prati C, Wendling D. Cryotherapy in inflammatory rheumatic diseases: a systematic review. Expert Rev Clin Immunol. 2014; 10:281–294. [PubMed: 24345205]

Hanssen MJ, Hoeks J, Brans B, van der Lans AA, Schaart G, van den Driessche JJ, Jorgensen JA, Boekschoten MV, Hesselink MK, Havekes B, et al. Short-term cold acclimation improves insulin sensitivity in patients with type 2 diabetes mellitus. Nat Med. 2015; 21:863–865. [PubMed: 26147760]

Hardie DG, Ross FA, Hawley SA. AMPK: a nutrient and energy sensor that maintains energy homeostasis. Nat Rev Mol Cell Biol. 2012; 13:251–262. [PubMed: 22436748]

Heng TS, Painter MW. Immunological Genome Project C. The Immunological Genome Project: networks of gene expression in immune cells. Nat Immunol. 2008; 9:1091–1094. [PubMed: 18800157]

Hotamisligil GS. Inflammation and metabolic disorders. Nature. 2006; 444:860–867. [PubMed: 17167474]

Hwang ES, White IA, Ho IC. An IL-4-independent and CD25-mediated function of c-maf in promoting the production of Th2 cytokines. Proc Natl Acad Sci U S A. 2002; 99:13026–13030. [PubMed: 12271139]

Kanneganti TD, Dixit VD. Immunological complications of obesity. Nat Immunol. 2012; 13:707–712. [PubMed: 22814340]

Kaplan MH, Schindler U, Grusby STSaMJ. Stat6 Is Required for Mediating Responses to IL-4 and for the Development of Th2 Cells. Immunity. 1996; 4:313–319. [PubMed: 8624821]

Kim CH. Molecular targets of FoxP3+ regulatory T cells. Mini reviews in medicinal chemistry. 2007; 7:1136–1143. [PubMed: 18045217]

Kim JM, Rasmussen JP, Rudensky AY. Regulatory T cells prevent catastrophic autoimmunity throughout the lifespan of mice. Nat Immunol. 2007; 8:191–197. [PubMed: 17136045]

Kissig M, Shapira SN, Seale P. SnapShot: Brown and Beige Adipose Thermogenesis. Cell. 2016; 166:258–258. e251. [PubMed: 27368105]

Kitoh A, Ono M, Naoe Y, Ohkura N, Yamaguchi T, Yaguchi H, Kitabayashi I, Tsukada T, Nomura T, Miyachi Y, et al. Indispensable role of the Runx1-Cbfbeta transcription complex for in vivo-suppressive function of FoxP3+ regulatory T cells. Immunity. 2009; 31:609–620. [PubMed: 19800266]

Klimek AT, Lubkowska A, Szygula Z, Fraczek B, Chudecka M. The influence of single whole body cryostimulation treatment on the dynamics and the level of maximal anaerobic power. International journal of occupational medicine and environmental health. 2011; 24:184–191. [PubMed: 21590430]

Kloting N, Fasshauer M, Dietrich A, Kovacs P, Schon MR, Kern M, Stumvoll M, Bluher M. Insulin-sensitive obesity. Am J Physiol Endocrinol Metab. 2010; 299:E506–515. [PubMed: 20570822]

Kretschmer K, Apostolou I, Hawiger D, Khazaie K, Nussenzweig MC, von Boehmer H. Inducing and expanding regulatory T cell populations by foreign antigen. Nat Immunol. 2005; 6:1219–1227. [PubMed: 16244650]

Kulak NA, Pichler G, Paron I, Nagaraj N, Mann M. Minimal, encapsulated proteomic-sample processing applied to copy-number estimation in eukaryotic cells. Nat Methods. 2014; 11:319–324. [PubMed: 24487582]

Lewis M, Tarlton JF, Cose S. Memory versus naive T-cell migration. Immunol Cell Biol. 2008; 86:226–231. [PubMed: 17998915]

Li H, Handsaker B, Wysoker A, Fennell T, Ruan J, Homer N, Marth G, Abecasis G, Durbin R. Genome Project Data Processing S. The Sequence Alignment/Map format and SAMtools. Bioinformatics. 2009; 25:2078–2079. [PubMed: 19505943]

Love MI, Huber W, Anders S. Moderated estimation of fold change and dispersion for RNA-seq data with DESeq2. Genome biology. 2014; 15:550. [PubMed: 25516281]

Lubkowska A, Szygula Z, Chlubek D, Banfi G. The effect of prolonged whole-body cryostimulation treatment with different amounts of sessions on chosen pro- and anti-inflammatory cytokines levels in healthy men. Scand J Clin Lab Invest. 2011; 71:419–425. [PubMed: 21574854]

MacIver NJ, Michalek RD, Rathmell JC. Metabolic Regulation of T Lymphocytes. Annual Review of Immunology. 2013; 31:259–283.

Maerten P, Shen C, Bullens DM, Van Assche G, Van Gool S, Geboes K, Rutgeerts P, Ceuppens JL. Effects of interleukin 4 on CD25+CD4+ regulatory T cell function. Journal of autoimmunity. 2005; 25:112–120. [PubMed: 16051465]

Malik M, van Gelderen EM, Lee JH, Kowalski DL, Yen M, Goldwater R, Mujais SK, Schaddelee MP, de Koning P, Kaibara A, et al. Proarrhythmic safety of repeat doses of mirabegron in healthy subjects: a randomized, double-blind, placebo-, and active-controlled thorough QT study. Clinical pharmacology and therapeutics. 2012; 92:696–706. [PubMed: 23149929]

Mathis D. Immunological goings-on in visceral adipose tissue. Cell Metab. 2013; 17:851–859. [PubMed: 23747244]

Medrikova D, Sijmonsma TP, Sowodniok K, Richards DM, Delacher M, Sticht C, Gretz N, Schafmeier T, Feuerer M, Herzig S. Brown adipose tissue harbors a distinct sub-population of regulatory T cells. PLoS One. 2015; 10:e0118534. [PubMed: 25714366]

Meissner F, Mann M. Quantitative shotgun proteomics: considerations for a high-quality workflow in immunology. Nat Immunol. 2014; 15:112–117. [PubMed: 24448568]

Michalek RD, Gerriets VA, Jacobs SR, Macintyre AN, MacIver NJ, Mason EF, Sullivan SA, Nichols AG, Rathmell JC. Cutting edge: distinct glycolytic and lipid oxidative metabolic programs are essential for effector and regulatory CD4+ T cell subsets. J Immunol. 2011; 186:3299–3303. [PubMed: 21317389]

Nguyen KD, Qiu Y, Cui X, Goh YP, Mwangi J, David T, Mukundan L, Brombacher F, Locksley RM, Chawla A. Alternatively activated macrophages produce catecholamines to sustain adaptive thermogenesis. Nature. 2011; 480:104–108. [PubMed: 22101429]

O'Sullivan D, Pearce EL. Targeting T cell metabolism for therapy. Trends Immunol. 2015; 36:71–80. [PubMed: 25601541]

Ortega-Molina A, Efeyan A, Lopez-Guadamillas E, Munoz-Martin M, Gomez-Lopez G, Canamero M, Mulero F, Pastor J, Martinez S, Romanos E, et al. Pten positively regulates brown adipose function, energy expenditure, and longevity. Cell Metab. 2012; 15:382–394. [PubMed: 22405073]

Panduro M, Benoist C, Mathis D. Tissue Tregs. Annu Rev Immunol. 2016; 34:609–633. [PubMed: 27168246]

Pillemer BB, Qi Z, Melgert B, Oriss TB, Ray P, Ray A. STAT6 activation confers upon T helper cells resistance to suppression by regulatory T cells. J Immunol. 2009; 183:155–163. [PubMed: 19535633]

Qiu Y, Nguyen KD, Odegaard JI, Cui X, Tian X, Locksley RM, Palmiter RD, Chawla A. Eosinophils and type 2 cytokine signaling in macrophages orchestrate development of functional beige fat. Cell. 2014; 157:1292–1308. [PubMed: 24906148]

Quelle FW, Shimoda K, Thierfelder W, Fischer C, Kim A, Ruben SM, Cleveland JL, Pierce JH, Keegan AD, Nelms K, et al. Cloning of murine Stat6 and human Stat6, Stat proteins that are tyrosine phosphorylated in responses to IL-4 and IL-3 but are not required for mitogenesis. Mol Cell Biol. 1995; 15:3336–3343. [PubMed: 7760829]

Rosen ED, Spiegelman BM. What we talk about when we talk about fat. Cell. 2014; 156:20–44. [PubMed: 24439368]

Rothwell NJ, Stock MJ. A role for brown adipose tissue in diet-induced thermogenesis. Nature. 1979; 281:31–35. [PubMed: 551265]

Rudra D, deRoos P, Chaudhry A, Niec RE, Arvey A, Samstein RM, Leslie C, Shaffer SA, Goodlett DR, Rudensky AY. Transcription factor Foxp3 and its protein partners form a complex regulatory network. Nat Immunol. 2012; 13:1010–1019. [PubMed: 22922362]

Rudra D, Egawa T, Chong MMW, Treuting P, Littman DR, Rudensky AY. Runx-CBF[beta] complexes control expression of the transcription factor Foxp3 in regulatory T cells. Nat Immunol. 2009; 10:1170–1177. [PubMed: 19767756]

Saito M, Okamatsu-Ogura Y, Matsushita M, Watanabe K, Yoneshiro T, Nio-Kobayashi J, Iwanaga T, Miyagawa M, Kameya T, Nakada K, et al. High incidence of metabolically active brown adipose tissue in healthy adult humans: effects of cold exposure and adiposity. Diabetes. 2009; 58:1526–1531. [PubMed: 19401428]

Sanchez-Guajardo V, Tanchot C, O'Malley JT, Kaplan MH, Garcia S, Freitas AA. Agonist-Driven Development of CD4+CD25+Foxp3+ Regulatory T Cells Requires a Second Signal Mediated by Stat6. The Journal of Immunology. 2007; 178:7550–7556. [PubMed: 17548589]

Sauer S, Bruno L, Hertweck A, Finlay D, Leleu M, Spivakov M, Knight ZA, Cobb BS, Cantrell D, O'Connor E, et al. T cell receptor signaling controls Foxp3 expression via PI3K, Akt, and mTOR. Proc Natl Acad Sci U S A. 2008; 105:7797–7802. [PubMed: 18509048]

Scheltema RA, Mann M. SprayQc: a real-time LC-MS/MS quality monitoring system to maximize uptime using off the shelf components. Journal of proteome research. 2012; 11:3458–3466. [PubMed: 22515319]

Schwanhäusser B, Busse D, Li N, Dittmar G, Schuchhardt J, Wolf J, Chen W, Selbach M. Global quantification of mammalian gene expression control. Nature. 2011; 473:337–342. [PubMed: 21593866]

Schweitzer LD, Comb WC, Bar-Peled L, Sabatini DM. Disruption of the Rag-Ragulator Complex by c17orf59 Inhibits mTORC1. Cell Rep. 2015; 12:1445–1455. [PubMed: 26299971]

Sehra S, Bruns HA, Ahyi AN, Nguyen ET, Schmidt NW, Michels EG, von Bulow GU, Kaplan MH. IL-4 is a critical determinant in the generation of allergic inflammation initiated by a constitutively active Stat6. J Immunol. 2008; 180:3551–3559. [PubMed: 18292582]

Serr I, Fürst RW, Achenbach P, Scherm MG, Gökmen F, Haupt F, Sedlmeier EM, Knopff A, Shultz L, Willis RA, et al. Type 1 diabetes vaccine candidates promote human Foxp3+Treg induction in humanized mice. Nature Communications. 2016; 7:10991.

Setiady YY, Coccia JA, Park PU. In vivo depletion of CD4+FOXP3+ Treg cells by the PC61 anti-CD25 monoclonal antibody is mediated by FcgammaRIII+ phagocytes. Eur J Immunol. 2010; 40:780–786. [PubMed: 20039297]

Shrestha S, Yang K, Guy C, Vogel P, Neale G, Chi H. Treg cells require the phosphatase PTEN to restrain TH1 and TFH cell responses. Nat Immunol. 2015; 16:178–187. [PubMed: 25559258]

Siegfried Ussar KYL, Dankel Simon N, Boucher Jeremie, Max-Felix Haering, Andre Kleinridders TT, Xue Ruidan, Macotela Yazmin, Cypess Aaron M, Yu-Hua Tseng GM, Ronald Kahn1 C. ASC-1, PAT2, and P2RX5 are cell surface markers for white, beige and brown adipocytes. Science Translational Medicine. 2014; 6:1–10.

Takasu T, Ukai M, Sato S, Matsui T, Nagase I, Maruyama T, Sasamata M, Miyata K, Uchida H, Yamaguchi O. Effect of (R)-2-(2-aminothiazol-4-yl)-4'-{2-[(2-hydroxy-2-phenylethyl)amino]ethyl} acetanilide (YM178), a novel selective beta3-adrenoceptor agonist, on bladder function. The Journal of pharmacology and experimental therapeutics. 2007; 321:642–647. [PubMed: 17293563]

Tyanova S. The Perseus computational platform for comprehensive analysis of (prote)omics data. Nature Methods. 2016 in press.

UniProt C. UniProt: a hub for protein information. Nucleic Acids Res. 2015; 43:D204–212. [PubMed: 25348405]

Vizcaino JA, Deutsch EW, Wang R, Csordas A, Reisinger F, Rios D, Dianes JA, Sun Z, Farrah T, Bandeira N, et al. ProteomeXchange provides globally coordinated proteomics data submission and dissemination. Nat Biotechnol. 2014; 32:223–226. [PubMed: 24727771]

von Boehmer H, Daniel C. Therapeutic opportunities for manipulating T(Reg) cells in autoimmunity and cancer. Nat Rev Drug Discov. 2013; 12:51–63. [PubMed: 23274471]

Webster KE, Walters S, Kohler RE, Mrkvan T, Boyman O, Surh CD, Grey ST, Sprent J. In vivo expansion of T reg cells with IL-2-mAb complexes: induction of resistance to EAE and long-term acceptance of islet allografts without immunosuppression. J Exp Med. 2009; 206:751–760. [PubMed: 19332874]

Yu XY, Lin SG, Wang XM, Liu Y, Zhang B, Lin QX, Yang M, Zhou SF. Evidence for coexistence of three beta-adrenoceptor subtypes in human peripheral lymphocytes. Clinical pharmacology and therapeutics. 2007; 81:654–658. [PubMed: 17361123]

Zhu J, Cote-Sierra J, Guo L, Paul WE. Stat5 activation plays a critical role in Th2 differentiation. Immunity. 2003; 19:739–748. [PubMed: 14614860]

Highlights

- Cold exposure or beta3-adrenergic stimulation induces T cell tolerance
- Beta3-adrenergic stimulation or cold exposure upregulates C17orf59 protein expression
- A Stat6/Pten axis links cold exposure with tolerance induction
- Foxp3^{+} regulatory T cells control brown adipose tissue metabolic function

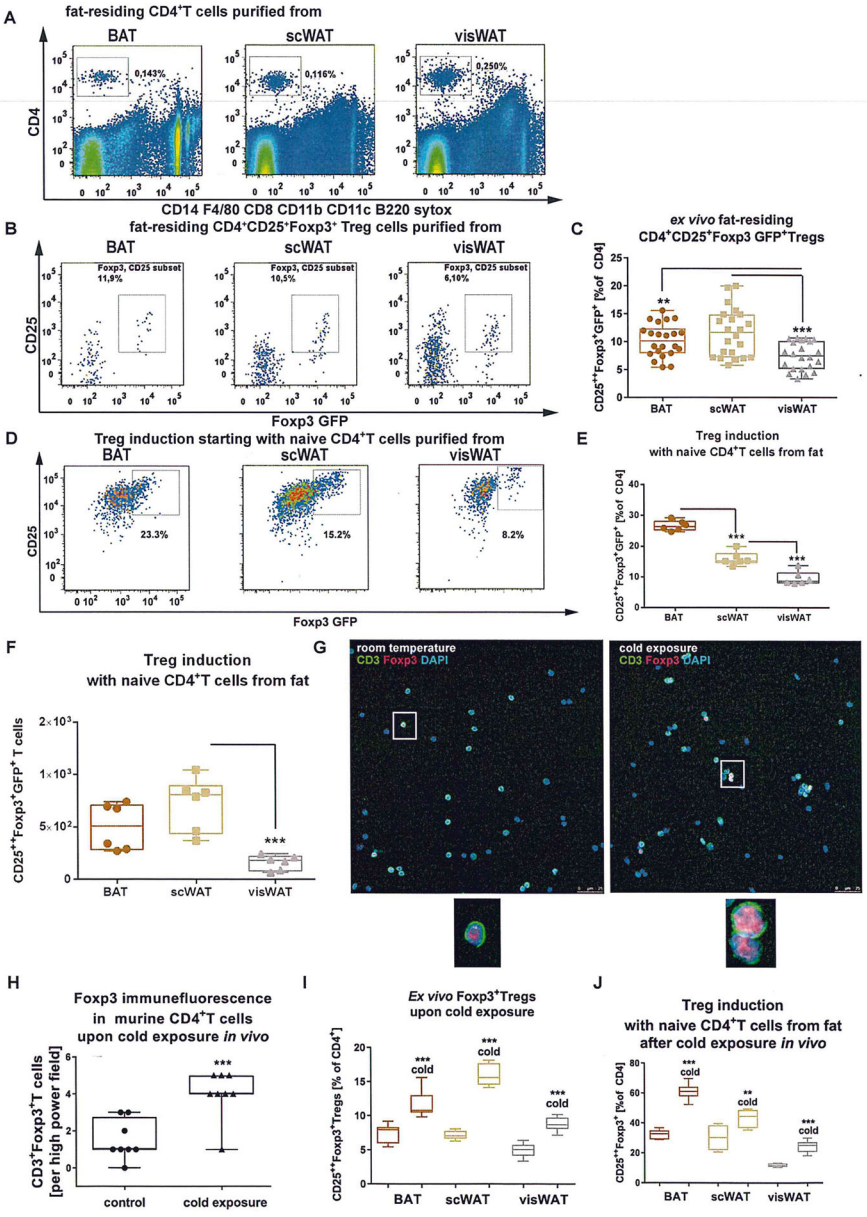

Figure 1. Frequencies and induction of regulatory T (Treg) cells in fat depots

(**A**) Representative FACS plots for the identification of fat-residing $CD4^+$T cells purified from BAT, scWAT or visWAT of young lean female Balbc Foxp3 GFP reporter mice. $CD4^+$T cells were gated on live $CD14^-$, $F4/80^-$, $CD8a^-$, $CD11b^-$, $CD11c^-$, B220, sytox and $CD4^+$. (**B**) Representative FACS plots for the identification of fat-residing $CD4^+CD25^+$Foxp3 GFP^+Tregs in BAT, scWAT or visWAT. (**C**) Box-and-whisker plots for frequencies of Foxp3 GFP^+ Tregs residing in fat-depots as indicated in B. n=22 per group from 5 independent experiments. (**D**) Representative FACS plots for *in vitro* Treg induction assays using limited TCR stimulation and naïve $CD4^+$T cells purified from different fat depots. (**E**) Box-and-whisker plots for *in vitro* Treg induction assays of fat-residing $CD4^+$T cells. n=6 per group. (**F**) Box-and-whisker plots of absolute Treg numbers obtained from Treg induction

experiments starting with identical numbers of naïve $CD4^+$T cells from respective fat-tissues. n=6 per group. (**G**) Representative confocal microscopy images of $CD4^+$T cells purified from mice upon *in vivo* cold exposure (4 days at 8°C). (**H**) $Foxp3^+CD3^+$T cells per high power field in samples from (G). n=8 per group. Data are shown as means±SEM from 2 independent experiments. (**I**) *Ex vivo* Treg frequencies purified from fat-depots of young Balbc mice upon *in vivo* cold exposure (24 h at 4°C). n=9 per group. (**J**) *In vitro* Treg induction assays of fat-residing naïve $CD4^+$T cells after *in vivo* cold-exposure (24 h at 4°C). n=6 per group. Data are presented as box-and-whisker plots with min and max values for data distribution, ** = $P<0.01$, *** = $P<0.001$.

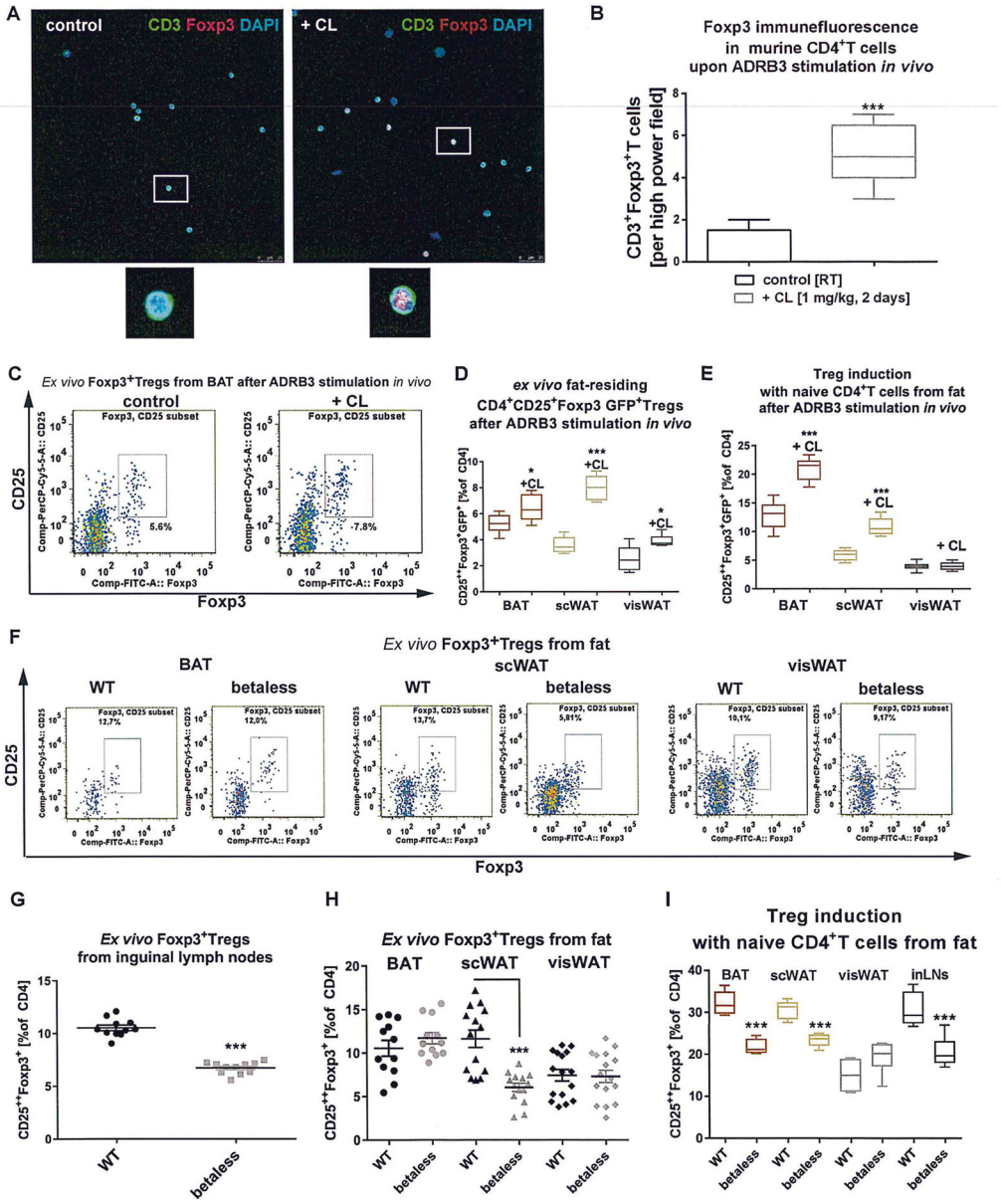

Figure 2. Beta-adrenergic stimulation promotes T cell tolerance

(**A**) Representative confocal microscopy images of CD4$^+$T cells purified from Balbc Foxp3 GFP reporter mice after *in vivo* treatment with CL (2 d, 1 mg/kg *i.p.*). (**B**) Foxp3$^+$CD3$^+$T cells per high power field in samples from (A). n=5 per group, P=0.0003. (**C**) Representative FACS plots for the identification of *ex vivo* CD4$^+$CD25$^+$Foxp3 GFP$^+$Tregs from BAT upon *in vivo* treatment with CL (3 d, 1 mg/kg *i.p.*). (**D**) Summary graph for *ex vivo* Treg frequencies purified from fat-depots of young Balbc mice as in (C). n=6 per group. (**E**) Summary graph for *in vitro* Treg induction assays with naïve CD4$^+$T cells from adipose tissues after *in vivo* treatment with CL (3 d, 1 mg/kg *i.p.*). n=6 per group. (**F**) Representative FACS plots for the identification of *ex vivo* CD4$^+$CD25$^+$Foxp3$^+$Tregs from fat depots of WT or mice lacking all three beta adrenergic receptors (betaless mice). (**G**) Summary graph for

ex vivo Treg frequencies purified from inguinal lymph nodes of WT or betaless mice. n=11 per group. (**H**) Summary graph for *ex vivo* Treg frequencies purified from fat depots of WT mice or betaless mice. n>12 per group. (**I**) Summary graph for *in vitro* Treg induction assays of naïve $CD4^+$T cells purified from fat depots or inguinal lymph nodes of WT or betaless mice. n=6 per group. Data are presented as box-and-whisker plots with min and max values for data distribution or as means±SEM. * = $P<0.05$, ** = $P<0.01$, *** = $P<0.001$.

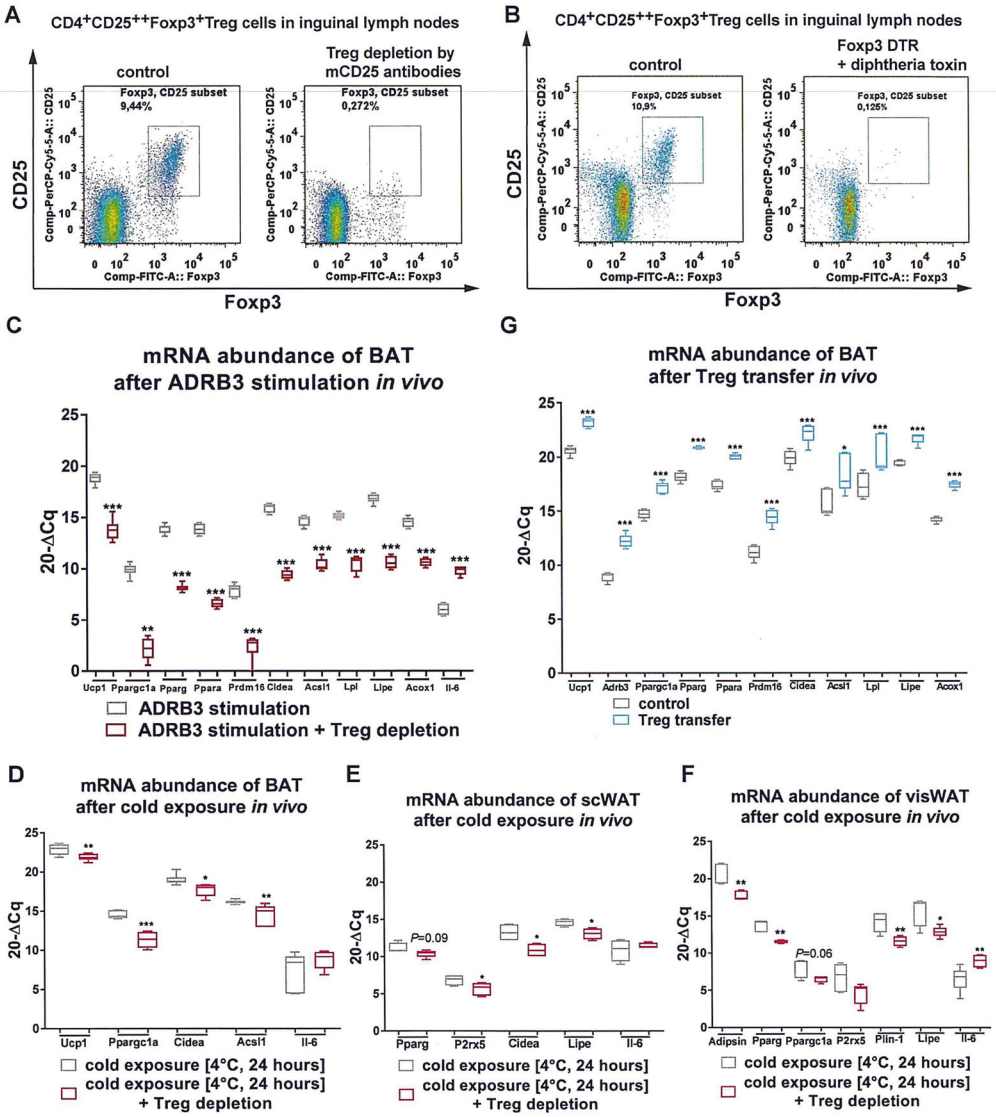

Figure 3. Role of Tregs induced by ADRB3 stimulation or cold exposure for adipose tissue function

(**A**) Representative FACS plots demonstrating Treg depletion efficacy in inguinal lymph nodes after 3 d of mCD25 antibody treatment. (**B**) Representative FACS plots demonstrating Treg depletion efficacy in inguinal lymph nodes 48 h after administration of diphtheria toxin. (**C**) mRNA expression of genes involved in BAT function upon treatment with CL *in vivo* in the presence or absence of Tregs. Tregs were depleted using anti-CD25 depleting antibodies. n=6 per group. (**D–F**) mRNA expression of genes involved in BAT (D), scWAT (E) and visWAT (F) function after cold exposure (4°C, 24h) in the presence or absence of Tregs. Tregs were depleted in Foxp3 DTR mice by administration of diphtheria toxin. n=6 per group. (**G**) In gain-of-function experiments, $CD4^+CD25^+Foxp3GFP^+$Tregs were adoptively transferred into congenic recipients. Analyses of BAT function by qPCR was performed 1 wk after transfer. n=6 per group. Data are presented as box-and-whisker plots with min and max values for data distribution. * = $P<0.05$, ** = $P<0.01$, *** = $P<0.001$.

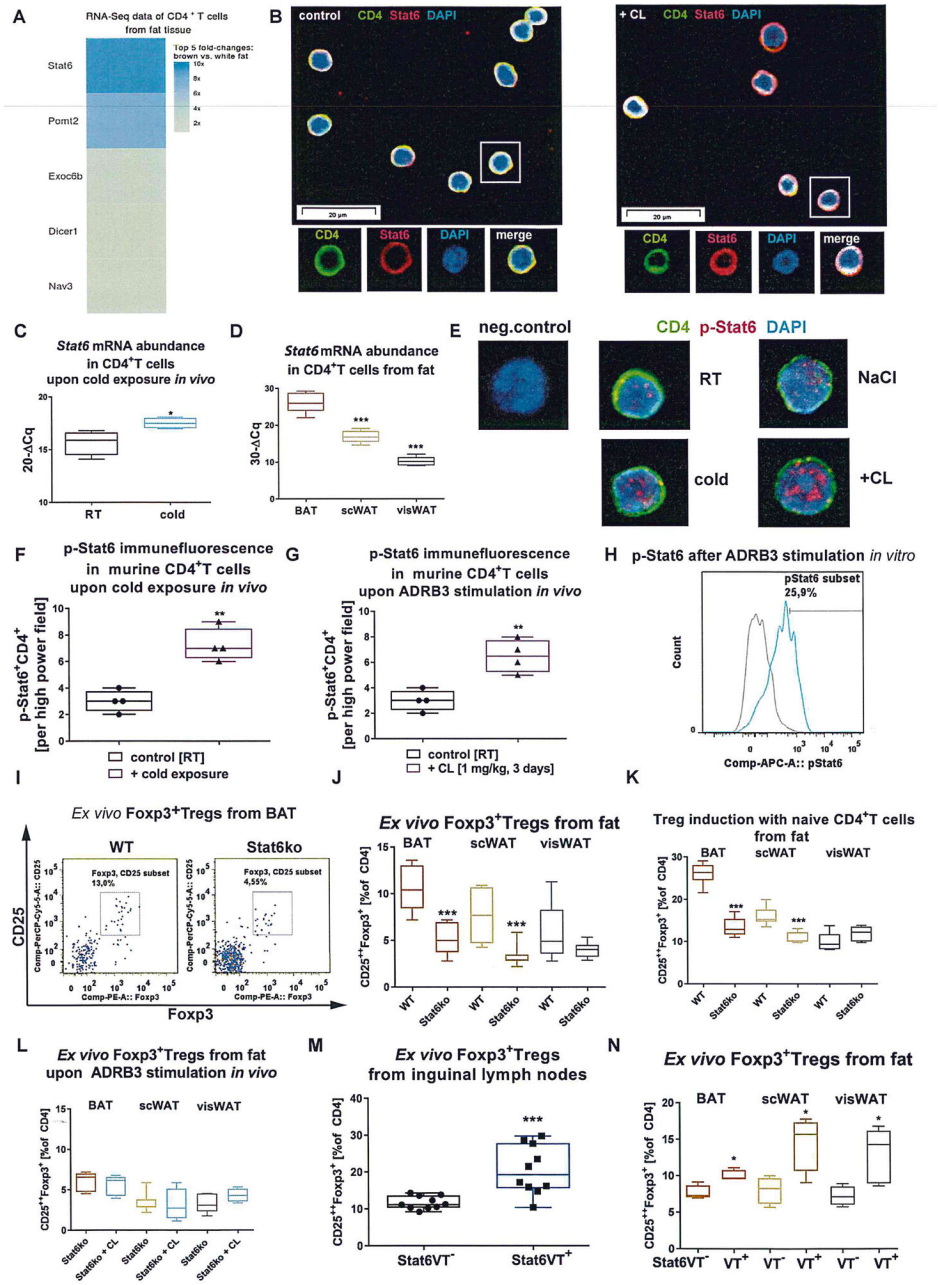

Figure 4. Role of Stat6 in T cell tolerance of fat-residing T cells

(**A**) Depicted are the top 5 fold-changes for upregulated genes in CD4$^+$T cells purified from brown vs. white fat by mRNA expression profiling. The cut-off for reading counts was set to 30 and pseudogenes have been manually removed. (**B**) Representative confocal microscopy images of CD4$^+$T cells purified from Balbc control mice or Balbc mice after *in vivo* treatment with CL (3 d, 1 mg/kg *i.p.*). (**C**) Quantitative RT-qPCR analyses of *Stat6* mRNA abundance in CD4$^+$T cells purified from Balbc mice upon cold exposure (1 wk, 8°C). n=4 mice per group from 2 independent experiments. (**D**) *Stat6* mRNA expression in CD4$^+$T cells purified from BAT, scWAT or visWAT of young lean Balbc mice. n=5 mice per group.

(**E**) Representative confocal microscopy images for p-Stat6 induction in $CD4^+$T cells from inguinal lymph nodes after CL treatment (3 d at 1 mg/kg *i.p.*) and *in vivo* cold exposure (4°C, 24 h). (**F**) Quantification of p-$Stat6^+CD4^+$T cells per high power field in samples from (E) after cold exposure. n=4 per group. (**G**) Quantification of p-$Stat6^+CD4^+$T cells per high power field in samples from (E) after CL treatment. n=4 per group. (**H**) Histogram of p-Stat6 detection in pre-activated $CD4^+$T cells after 10 nM CL stimulation for 15 min *in vitro*. (**I**) Representative FACS plots for the identification of *ex vivo* $CD4^+CD25^+Foxp3^+$Tregs from BAT of WT or Stat6ko mice. (**J**) Summary graph for *ex vivo* Treg frequencies purified from fat depots of WT mice or Stat6ko mice. n=10 per group. (**K**) Summary graph for *in vitro* Treg induction assays of naïve $CD4^+$T cells purified from fat depots of WT or Stat6ko mice. n=6 per group. (**L**) Summary graph for *in vitro* Treg induction assays of naïve $CD4^+$T cells purified from BAT, scWAT and visWAT Stat6ko mice that were treated with vehicle or CL (3 d, 1 mg/kg) *in vivo*. (**M**) Representative FACS blots for *ex vivo* Treg frequencies purified from inguinal lymph nodes of WT mice or mice with constitutively active Stat6 (Stat6VT mice). n=10 per group. (**N**) Summary graph for *ex vivo* $CD4^+CD25^+Foxp3^+$ Treg frequencies purified from fat depots of $Stat6VT^+$ or $Stat6VT^-$ mice. n=4 per group. Data are presented as box-and-whisker plots with min and max values for data distribution. * = $P<0.05$, ** = $P<0.01$, *** = $P<0.001$.

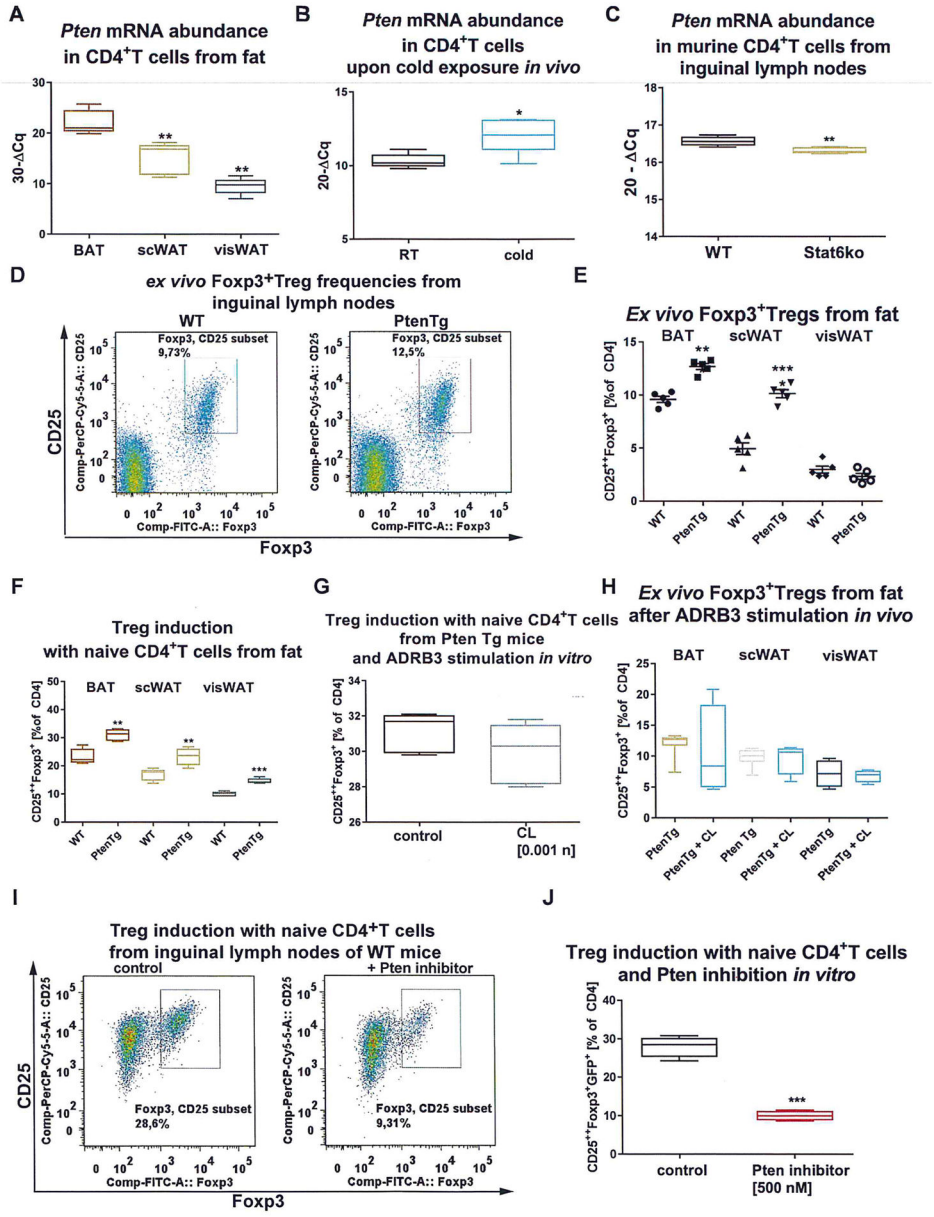

Figure 5. Role of Pten in T cell tolerance of fat-residing CD4$^+$T cells

Quantitative RT-qPCR analyses of *Pten* mRNA abundance in (**A**) CD4$^+$T cells purified from BAT, scWAT or visWAT of young lean Balbc animals. n=5 per group, (**B**) CD4$^+$T cells purified from inguinal lymph nodes after *in vivo* cold exposure of Balbc animals. n=5 per group and in (**C**) CD4$^+$T cells purified from inguinal lymph nodes of Stat6ko animals, n=4 per group. (**D**) Representative FACS plots identifying *ex vivo* CD4$^+$CD25$^+$Foxp3$^+$Tregs from inguinal lymph nodes of WT or mice transgenetically-overexpressing *Pten* (PtenTg animals). (**E**) Summary graph for the identification of *ex vivo* CD4$^+$CD25$^+$Foxp3$^+$Tregs purified from BAT, scWAT or visWAT of WT or PtenTg mice. n=5 per group. (**F**) Summary graph for *in vitro* Treg induction assays using limited TCR stimulation of naïve CD4$^+$T cells purified from fat depots of WT or PtenTg animals. n=6 per group. (**G**) Summary graph for *in*

vitro Treg induction assays using limited TCR stimulation of naïve $CD4^+$T cells of PtenTg animals in the presence or absence of ADRB3 stimulation [0.001 nM CL]. n=5 per group. (**H**) *Ex vivo* Treg frequencies purified from fat-depots of PtenTg mice upon *in vivo* ADRB3 stimulation (3 d, 1 mg/kg CL). n=8 for PtenTg control group and n=4 for PtenTg + CL group. (**I**) Representative FACS plots for *in vitro* Treg induction assays with or without Pten inhibitor (500 nM) using naïve $CD4^+$T cells purified from inguinal lymph nodes of WT mice. (**J**) Summary graph of Pten inhibition for *in vitro* Treg induction assays of naïve $CD4^+$T cells purified from inguinal lymph nodes of WT animals. n=4 per group from 2 independent experiments. Data are presented as box-and-whisker plots with min and max values for data distribution or as means±SEM. * = $P<0.05$, ** = $P<0.01$, *** = $P<0.001$.

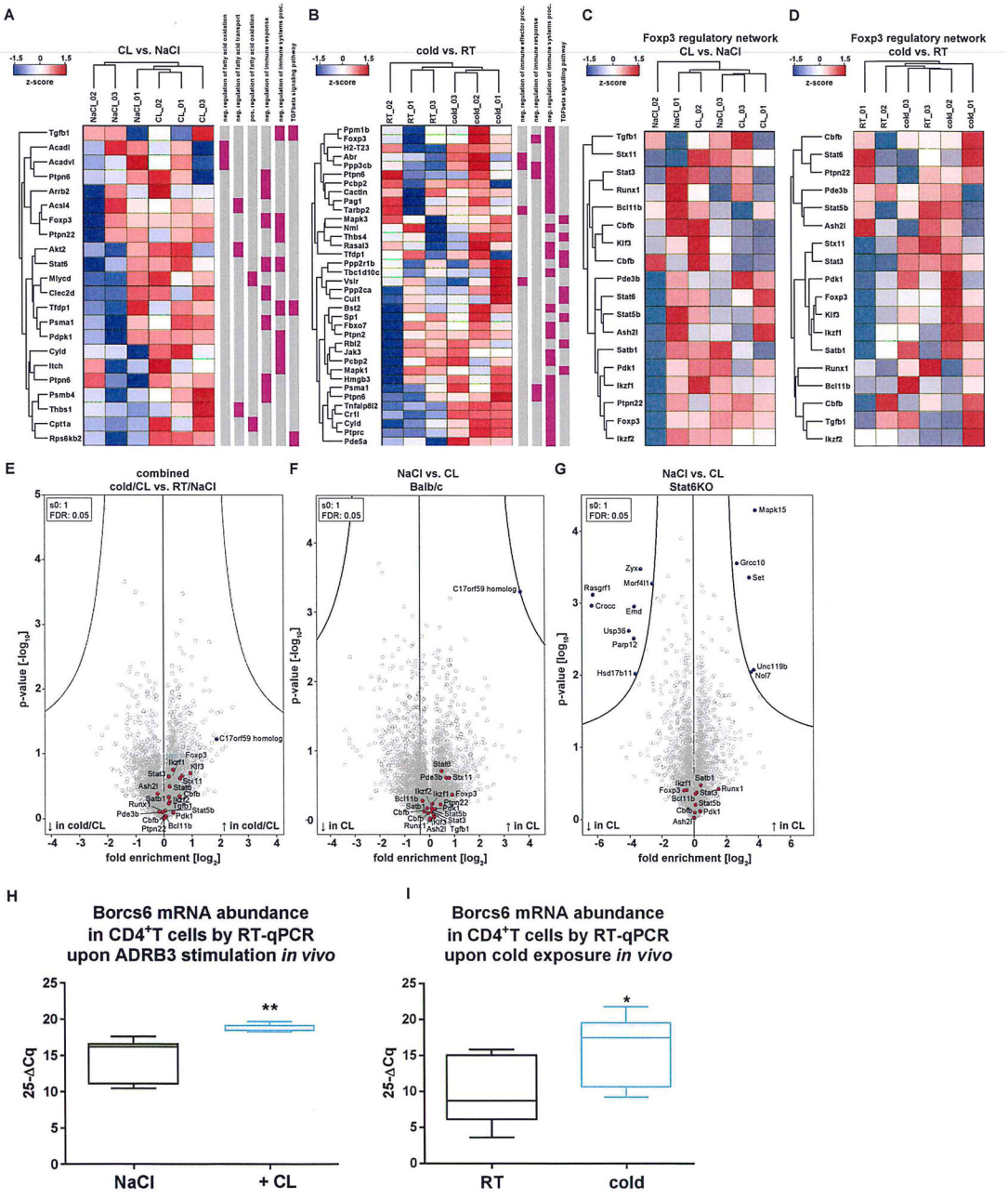

Figure 6. Cold exposure or ADRB3 stimulation induces a tolerogenic proteome signature in CD4^{+}T cells

(**A+B**) Proteins associated with selected GeneOntology terms Biological Function (GOBP) were grouped using unsupervised hierarchical clustering of the z-scored MaxLFQ-intensities across the indicated experimental groups; CL vs. NaCl (A) and cold vs. RT (B). GOBP annotations are depicted in purple. (**C+D**) Proteins associated with the Foxp3 regulatory network were grouped using unsupervised hierarchical clustering of the z-scored MaxLFQ-intensities across the indicated experimental groups; CL vs. NaCl (C) and cold vs. RT (D). (**E–G**) Combined volcano plot of the pairwise comparison between CD4^{+}T cell proteomes purified from cold/CL- vs. RT/NaCl-treated mice (E), NaCl- vs. CL-treated mice (F) and

NaCl- vs. CL-treated Stat6ko mice (G). Expression fold changes (t-test difference, $\log_2$) were calculated and plotted against the t-test p-value ($-\log_{10}$). Proteins associated with Foxp3 regulatory networks (red) and the C17orf59 homologue (blue) are highlighted. Their position on the right side of the plot indicates a higher abundance upon cold/CL- (E) or CL-treatment (F+G). (**H+I**) Quantitative RT-qPCR analyses of *Borcs6* mRNA abundance in $CD4^+$T cells purified from mice after *in vivo* ADRB3 stimulation (H) or cold exposure (I). n=5 mice per group. Data are presented as box-and-whisker plots with min and max values for data distribution. * = $P<0.05$, ** = $P<0.01$.

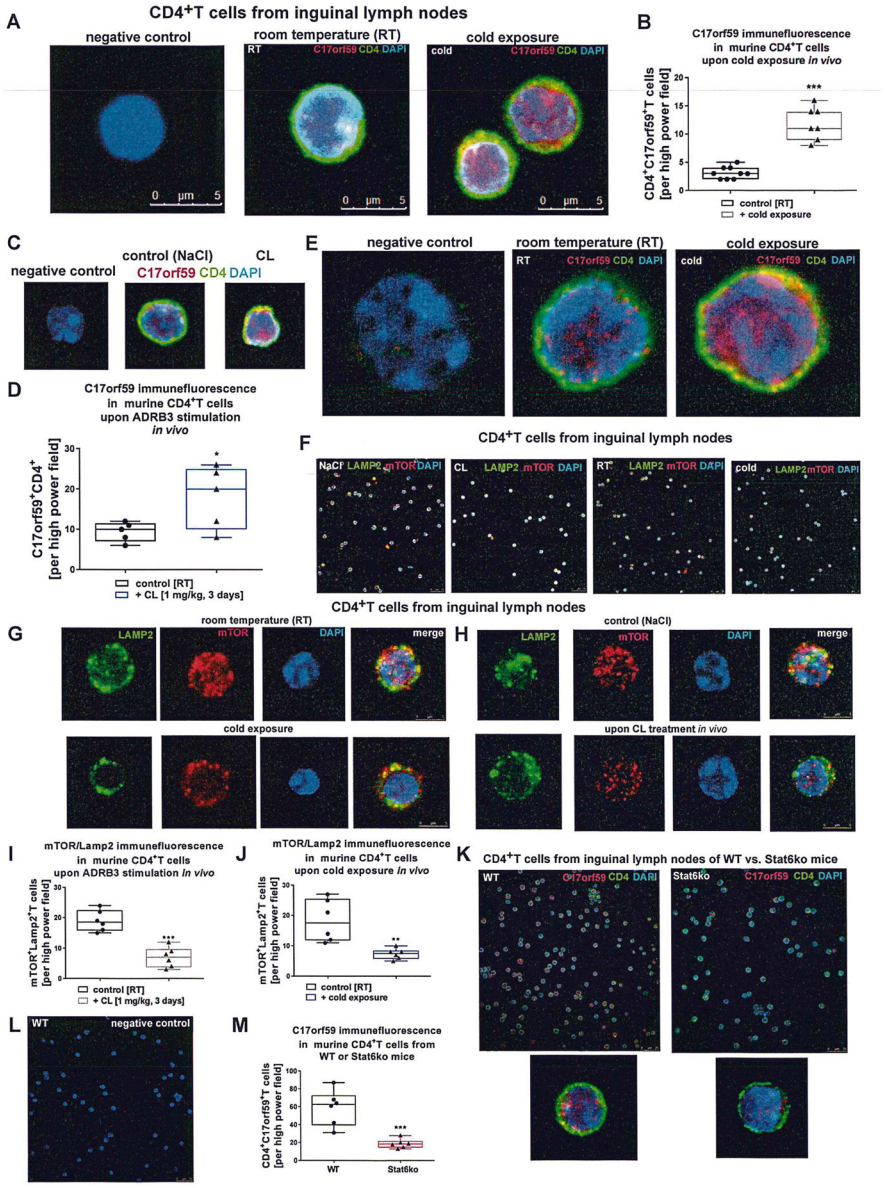

Figure 7. ADRB3 stimulation or cold-exposure increases C17orf59 protein expression in CD4$^+$T cells

(**A**) Representative confocal microscopy images for C17orf59 expression of CD4$^+$T cells purified from inguinal lymph nodes of mice exposed to cold *in vivo* (24 h, 4°C). (**B**) C17orf59$^+$CD4$^+$T cells per high power field in samples from CD4$^+$T cells from (A). n=9 for control group at room temperature and n=6 for group at 4°C. (**C**) Representative high magnification confocal images for C17orf59 expression of CD4$^+$T cells purified from inguinal lymph nodes of mice subjected to ADRB3 stimulation (3 d, 1 mg/kg CL). (**D**) C17orf59$^+$CD4$^+$T cells per high power field in samples from (C). n=5 per group. (**E**) Stimulated emission depletion (STED) microscopy of cytoplasmatic C17orf59 expression in CD4$^+$T cells purified from inguinal lymph nodes of mice upon cold exposure. (**F**) Representative confocal microscopy images for Lamp2 and mTOR expression in CD4$^+$T

cells purified from inguinal lymph nodes of mice subjected to ADRB3 stimulation or cold exposure *in vivo*. (**G+H**) Single cell magnifications and depiction of single stainings of samples from (F) after cold exposure (G) or ADRB3 stimulation (H). (**I**) $mTOR^{+}Lamp2^{+}T$ cells per high power field in samples from $CD4^{+}T$ cells purified from inguinal lymph nodes of mice subjected to CL (3 d, 1 mg/kg CL). n=6 per group. (**J**) $mTOR^{+}Lamp2^{+}T$ cells per high power field in samples from $CD4^{+}T$ cells purified from inguinal lymph nodes of mice subjected to cold exposure (24 h, 4°C) *in vivo*. n=6 per group. (**K**) Representative confocal microscopy images for C17orf59 expression in $CD4^{+}T$ cells purified from inguinal lymph nodes of WT or Stat6ko mice. (**L**) Negative staining control of C17orf59. Shown are stainings with secondary antibody in the absence of primary antibodies using $CD4^{+}T$ cells from WT mice. Data are presented as box-and-whisker plots with min and max values for data distribution. * = $P<0.05$, ** = $P<0.01$, *** = $P<0.001$.